A Solid–Liquid Composite Lubricating "Nano-Snowboard" for Long-Acting Treatment of Osteoarthritis

Wenjie Qiu, Weiwei Zhao,* Ludan Zhang, Haimang Wang, Ningyu Li, Kexin Chen, Hongyu Zhang,* and Yuguang Wang*

Osteoarthritis is a chronic inflammatory disease characterized by cartilage degeneration. Anti-inflammatory therapy has limited effects, and effective reduction of cartilage wear through lubrication is essential. In vivo stability and lubricity of commercial lubricants are insufficient, leading to failure of lubricating treatment and progression of osteoarthritis. To address these issues, new therapeutic methods combining anti-inflammation and stable high-performance lubrication are developed. Inspired by the sliding mechanism of snowboards, a "nano-snowboard" by modifying molybdenum disulfide (MoS$_2$) with a biomimetic phospholipid polymer poly (dopamine methacrylamide-co-2-methacryloyloxyethyl phosphorylcholine) (PDMPC) and loading anti-inflammatory drug diclofenac sodium (DS), namely MoS$_2$-PDMPC-DS, has been synthesized. MoS$_2$ with a 2D layered structure and photothermal properties, serves as solid lubricant and drug carrier. Meanwhile, the modification of PDMPC on the surface of MOS$_2$ avoids the oxidative denaturation of MoS$_2$ in a physiological environment, forming solid–liquid composite lubrication and improving the lubricity and stability of MoS$_2$ in the joint cavity. In vitro and in vivo experiments show that MoS$_2$-PDMPC-DS can stay in the joint cavity for more than one week and exert long-lasting lubrication and anti-inflammatory effects to treat osteoarthritis effectively. This solid–liquid composite lubricating nano-snowboard provides a new idea for synergistic anti-inflammatory and lubricating treatment of osteoarthritis.

1. Introduction

Osteoarthritis, as a chronic joint disease, is characterized mainly by synovial inflammation and cartilage degeneration.[1–3] Osteoarthritis affects more than 300 million people worldwide, and knee osteoarthritis is a major factor of disability in middle-aged and elderly people.[4–6] Osteoarthritis is accompanied by symptoms such as severe pain and dysfunction, and its pathological process is irreversible. Osteoarthritis seriously affects the daily life of patients and places a great burden on personal economy and social medical security. Moreover, this burden is widely believed to continue to increase as the population ages.[6–8]

As a routine clinical treatment, non-steroidal anti-inflammatory drugs (NSAIDs) achieve mainly anti-inflammatory and analgesic effects by inhibiting the activity of selective cyclooxygenase-2 (COX-2).[9–11] However, due to the low drug-usage rate, short residence time, large drug dosage and certain toxic side effects (especially for the gastrointestinal tract), the therapeutic effect of NSAIDs is limited.[12–15] Nanodrug delivery systems such as mesoporous silica nanoparticles, liposomes, and metal nanoparticles have been used as a novel therapeutic modality for osteoarthritis and have achieved significantly better efficacy than that of traditional oral anti-inflammatory drugs.[16–18] However, anti-inflammatory therapy alone has limited efficacy in relieving osteoarthritis and improving joint function.[14] As another important treatment method, intra-articular lubrication mainly relieves osteoarthritis symptoms and improves joint function by reducing joint abrasion.[19] However, existing commercial liquid lubricants,

W. Qiu, L. Zhang, N. Li, K. Chen, Y. Wang
Center of Digital Dentistry/ Department of Prosthodontics
National Center of Stomatology
National Clinical Research Center for Oral Diseases
National Engineering Laboratory for Digital and Material Technology of Stomatology
Beijing Key Laboratory of Digital Stomatology
NHC Research Center of Engineering and Technology for Computerized Dentistry
Peking University School and Hospital of Stomatology
Beijing 100081, China
E-mail: wangyuguang@bjmu.edu.cn

W. Zhao, H. Wang, H. Zhang
State Key Laboratory of Tribology
Department of Mechanical Engineering
Tsinghua University
Beijing 100084, China
E-mail: zhaoweiwei@sdu.edu.cn; zhanghyu@tsinghua.edu.cn

W. Zhao
Department of Biomaterials
School and Hospital of Stomatology
Cheeloo College of Medicine
Shandong University& Shandong Provincial Key Laboratory of Oral Tissue Regeneration & Shandong Engineering Laboratory for Dental Materials and Oral Tissue Regeneration
Jinan 250012, China

such as hyaluronic acid, still have obvious problems in practical application. The first problem is stability. Due to the presence of hyaluronidase, hyaluronic acid will quickly be degraded and cleared in the body, therefore the hyaluronic acid cannot continue to perform a lubricating function.[20] The second problem is effectiveness. At a high shear rate of joint motion, hyaluronic acid undergoes a "shear thinning" behavior, resulting in a decrease in viscosity and lubricating performance.[21] Studies have shown that failure of joint lubrication leads to further degradation of cartilage and aggravation of osteoarthritis.[22–24] Therefore, a new treatment method is urgently required to overcome the above problems and achieve effective anti-inflammatory effects and stable, high-performance lubrication.

Molybdenum disulfide (MoS_2), as a 2D nanomaterial, is highly sensitive to near-infrared (NIR) lasers and has good NIR laser absorption and photothermal conversion capabilities.[25–27] In addition, its special specific surface area and void structure make it an excellent carrier for drug loading and surface functionalization.[28–30] These advantages endow MoS_2 broad application potential in the field of biomedicine and MoS_2 has become a research hotspot in recent years. Zhao et al. used the photoresponsive properties of MoS_2 to control the release of anti-inflammatory drugs for the treatment of osteoarthritis and achieved good anti-inflammatory effects.[31] In addition, as a typical layered compound, the sulfur (S) atoms and the molybdenum (Mo) atoms in the MoS_2 layer are tightly bound by covalent bonds, and the van der Waals force is the main force between the layers, which makes the layers prone to interlayer slippage and has a low friction coefficient (COF). Therefore, MoS_2 has excellent solid lubricating properties and is widely used in industrial fields such as bearings and slide rails under high loads.[32] Unfortunately, in physiological environment, MoS_2 can be oxidized to water-soluble substances (such as MoO_4^{2-}), making its layered structure collapse and the nanosheets easily removed by the body.[33–35] Therefore, solving the stability problem of MoS_2 in the physiological environment is the key issue to enabling MoS_2 to achieve long-term service in vivo.

Whether it is liquid lubrication represented by hyaluronic acid or solid lubrication represented by MoS_2, it is difficult to fulfill stable, long-lasting and reliable requirements in harsh physiological environments such as joints.[36] In industry, to compensate for the limitations of a single lubrication method, solid–liquid composite lubrication technology (that is, adding a layer of liquid lubricant to the surface of the solid lubricating film) is often used to convert the original solid–solid contact into a solid–liquid contact, reducing component wear and achieving more durable and efficient lubrication.[37–39] Different from the macroscopic composite mode of solid film-liquid lubricant common in industry, Ma et al. uniformly dispersed nanoscale single-layer graphene and multilayer graphite materials into glycerol and found that graphene and graphite retained the characteristics of solid lubricants in this system.[40] This phenomenon inspired us to modify the surface of graphene-like nano-MoS_2 material with a uniform liquid lubricating coating and inject it into the joint cavity. Macroscopically, the solid–solid friction between the articular surfaces is transformed into solid–liquid friction between the articular surfaces and the liquid lubricant, while microscopically, the interlayer solid–solid friction of MoS_2 is transformed into liquid–liquid friction between the hydration layers on the surface of the MoS_2. Whether this method can achieve the enhanced composite lubrication effect on macroscopic and microscopic scale synergistically, and avoid direct contact between MoS_2 and body fluids, thereby greatly improving the lubricity and stability of MoS_2, remains to be determined.

In this study, we apply the technique of solid–liquid composite lubrication to the biomedical field for the first time and constructed a "nano-snowboard", namely MoS_2-PDMPC-DS, which is composed mainly of MoS_2 nanosheets with PDMPC modified on its surface and loaded with DS. In the nanosheets, PDMPC has the same $N^+(CH_3)_3$ and PO_4^- functional groups as phosphatidylcholine lipids in cartilage, which can interact with surrounding water molecules through the "hydration lubrication mechanism" to form a hydrated layer and behave in the fluid state when subjected to shear forces, enabling joints to bear high pressure.[41,42] We modify PDMPC on the surface of MoS_2 nanosheets to form a hydration layer and stabilize the internal structure of MoS_2. Together they play a solid–liquid composite lubrication role, similar to the sliding mechanism in which a water layer is formed between the snowboard and snow, thus greatly reducing friction. At the same time, MoS_2 nanosheets are loaded with DS, a kind of NSAIDs, to achieve long-lasting relief of inflammation in joints. The synthesis schematic is shown in **Scheme 1**a. MoS_2-PDMPC-DS nanosheets were injected into the joint cavity of the rats, which can play a solid–liquid composite lubrication role and effectively reduce the COF between the articular cartilage surfaces. When the joint cavity is irradiated with NIR laser, the MoS_2-PDMPC-DS in the joint cavity undergoes photothermal conversion to promote the release of DS, and inhibit the secretion of inflammatory factors by macrophages, thus achieving anti-inflammatory and analgesic effects (Scheme 1b). In addition, MoS_2-PDMPC-DS have a long-lasting stable presence in the joint cavity and exert dual effects of lubrication and anti-inflammation. MoS_2-PDMPC-DS, as a novel solid–liquid composite lubricating drug carrier system, provide a new idea for the treatment of osteoarthritis. It is anticipated that this solid–liquid composite lubricating drug carrier system can be used as a potential intra-articular injection approach to effectively treat osteoarthritis.

2. Results and Discussion

2.1. Synthesis and Characterization of MoS_2-PDMPC-DS

Transmission electron microscopy (TEM) and high-resolution TEM (HRTEM) are employed to characterize the structure of MoS_2 nanosheets. TEM and HRTEM (**Figure 1**a; Figure S1a, Supporting Information) images show that MoS_2 exhibits a layered structure of monolayer or multilayer stacking, which proves that we have successfully synthesized MoS_2 nanosheets. Furthermore, the (100) and (110) crystallographic planes in the selected area electron diffraction (SAED) image indicate that the exfoliated MoS_2 nanosheets are in the 2H crystal phase. The elemental spectrum (Figure 1b) and energy dispersive X-ray (EDX) analysis (Figure 1c) demonstrate the presence
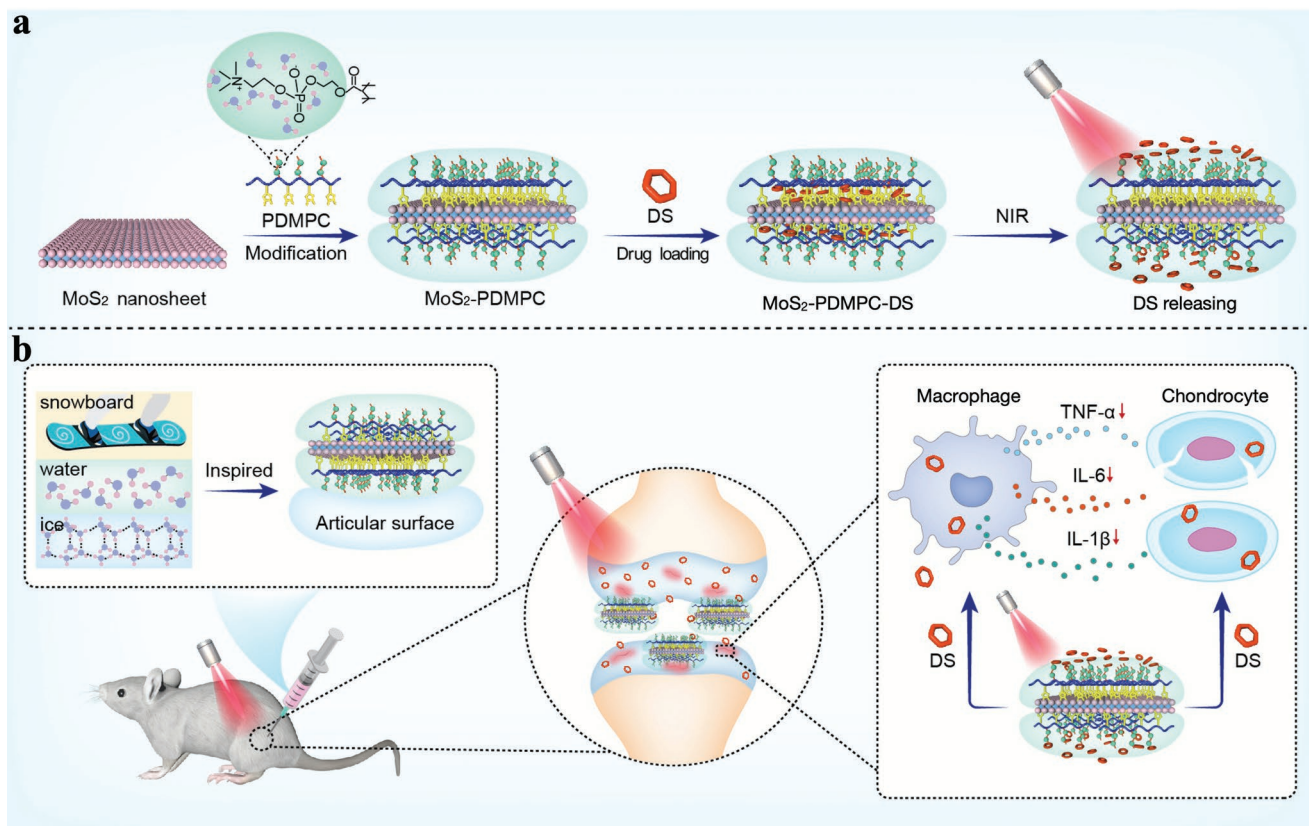
Scheme 1. Schematic illustration of molybdenum disulfide drug delivery system. a) Synthesis of MoS₂-PDMPC-DS and its drug release and lubrication function under NIR laser irradiation. b) Intra-articular injection of MoS₂-PDMPC-DS with NIR laser irradiation to achieve lubricating and anti-inflammatory effects in the synergetic treatment of osteoarthritis based on enhanced lubrication and sustained drug release.

of Mo and S element, confirming the existence of MoS_2 nanosheets. The powder X-ray diffraction (XRD) spectrum (Figure 1d) reveals the sheet-like structure of MoS_2, which is in accordance with the HRTEM results. The Raman spectra (Figure S1b, Supporting Information) show the corresponding in-plane (E_{2g}^1) and out-of-plane (A_{1g}) vibrational modes of the layered 2H-MoS_2 at 383 and 408 cm^{-1}. The above characterization shows that MoS_2 nanosheets have been successfully synthesized. Zeta potential, Fourier transform infrared (FTIR) spectroscopy, and ultraviolet-visible (UV–vis) spectroscopy are conducted to evaluate the successful surface modification and drug loading process. The absolute zeta potential value of MoS_2 nanosheets is decreased after PDMPC modification and DS loading process (Figure 1e). The FTIR diagram of MoS_2-PDMPC shows the characteristic absorption peak of P—O and P=O at 954 and 1229 cm^{-1}, demonstrating the successful modification of PDMPC on MoS_2. MoS_2-PDMPC-DS exhibits a characteristic peak of chlorinated benzene bending absorption peak at 1574 cm^{-1} (Figure 1f). The FTIR results prove that MoS_2 nanosheets have been successfully modified with PDMPC and DS. The size distribution results (Figure 1g) show that the particle size of MoS_2 nanosheets is ≈200 nm and the size distribution of MoS_2-PDMPC and MoS_2-PDMPC-DS is ≈400 nm. The increased hydrodynamic diameter of nanosheets is due to the modification of PDMPC and DS. UV–vis (Figure 1h) results show that PDMPC and DS have strong absorption peaks at 276 and

280 nm, respectively. Compared with MoS_2, MoS_2-PDMPC-DS has obvious absorption peaks at 276 and 280 nm, which is caused by PDMPC and DS modification on the surface of MoS_2. Moreover, MoS_2 shows a marked absorption peak in the near-infrared region, confirming the photothermal conversion capability under NIR irradiation.

2.2. Lubrication Performance of MoS₂-PDMPC

To investigate the lubrication properties of MoS_2-PDMPC, we monitored the COF values of MoS_2-PDMPC at different concentrations and loading forces, and the COF values of unmodified MoS_2 nanosheets are also tested for comparison (**Figure 2**a–c). Figure 2a shows that the MoS_2 nanosheets themselves have a certain lubricity performance. The COF of MoS_2 nanosheets is between 0.06–0.07 when the loading force varies from 35 to 55 MPa, which is significantly lower than the COF of H_2O. However, MoS_2 nanosheets cannot fulfill the needs of the lubrication of joints, as MoS_2 crystals can be oxidized to water-soluble substances in the physiological environment, which will cause them to undergo structural deterioration and weaken their lubrication properties.[43] The COF value of MoS_2-PDMPC is between 0.03–0.04, which indicates that PDMPC successfully enhances the lubrication performance of MoS_2 nanosheets by 50%. Figure 2b shows that the COF values of MoS_2-PDMPC
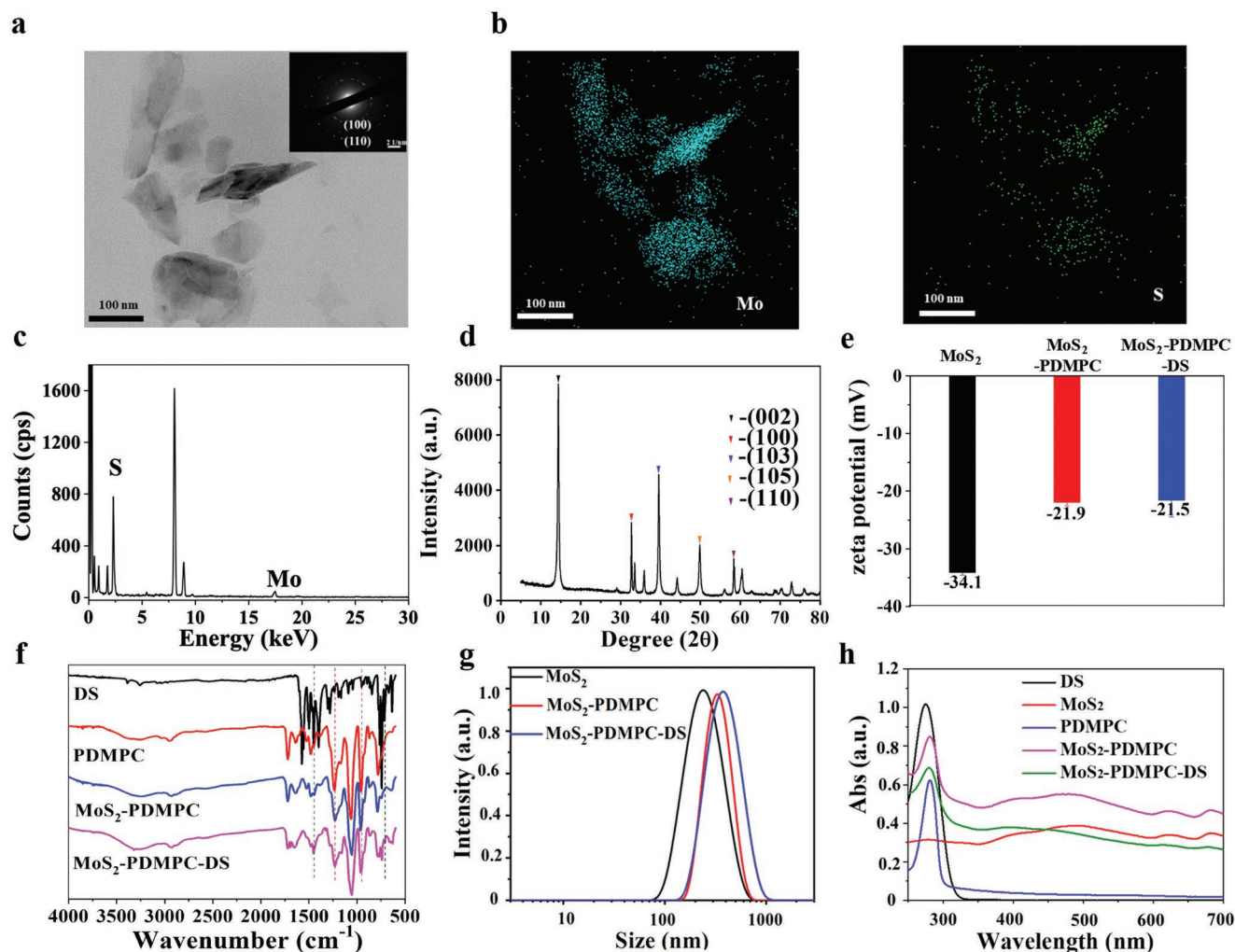
Figure 1. Material characterization. a) HRTEM and SAED images of MoS_2 nanosheets. b) Elemental analysis of MoS_2 nanosheets. c) EDX spectrum of MoS_2 nanosheets. d) XRD spectrum of MoS_2 nanosheets. e) Zeta potential of MoS_2, MoS_2-PDMPC, and MoS_2-PDMPC-DS nanosheets. f) FTIR spectra of DS, PDMPC, MoS_2-PDMPC, and MoS_2-PDMPC-DS. g) Size distribution of MoS_2, MoS_2-PDMPC, and MoS_2-PDMPC-DS. h) UV–vis spectra of DS, MoS_2, PDMPC, MoS_2-PDMPC, and MoS_2-PDMPC-DS.

slightly decrease with increasing concentration. The excellent lubricating properties of MoS_2-PDMPC are attributed mainly to the fact that PDMPC is modified on the surface of MoS_2 nanosheets, giving it the dual properties of solid and liquid lubricants. The lubrication mechanism is shown in Figure 2d. The $N^+(CH_3)_3$ and PO_4^- functional groups in PDMPC attract many water molecules through the ion–dipole interaction and form a compact hydration layer surrounding the charges. MoS_2 nanosheets modified with PDMPC form a hydration layer on the surface of the nanosheets, endowing the solid lubricant with liquid lubrication effect. After MoS_2-PDMPC is injected into the joint cavity, a low COF will be obtained through hydration lubrication mechanism. MoS_2-PDMPC exhibits excellent lubricity when subjected to shear forces of joint motion. The hydration layer formed by PDMPC can protect the solid lubricating properties of MoS_2, resist the strong shear force during joint movement, and enable the nanosheets to exert solid–liquid composite lubricating properties.

2.3. Photothermal Performance of MoS_2-PDMPC-DS

The photothermal performance of MoS_2 is very important for its application in biomedicine. MoS_2 and MoS_2-PDMPC-DS are irradiated with an 808 nm NIR laser to evaluate the photothermal performance. Compared with the phosphate-buffered saline (PBS) group, the temperatures of MoS_2 and MoS_2-PDMPC-DS are obviously increased under NIR laser irradiation. After irradiation for 10 min, the temperature of MoS_2 and MoS_2-PDMPC-DS increases from 27 to 42.0 and 41.9 °C, respectively, and tends to achieve a plateau (**Figure 3**a,b). Figure 3c,d shows that MoS_2-PDMPC-DS has excellent photothermal conversion performance, and the photothermal conversion efficiency of MoS_2-PDMPC-DS shows a positive correlation with the concentration and the power density of the NIR laser. Figure 3e shows that the higher the concentration of MoS_2-PDMPC-DS under NIR laser irradiation with a constant power, the higher the temperature. In addition, laser on/off experiments prove that MoS_2-PDMPC-DS has excellent
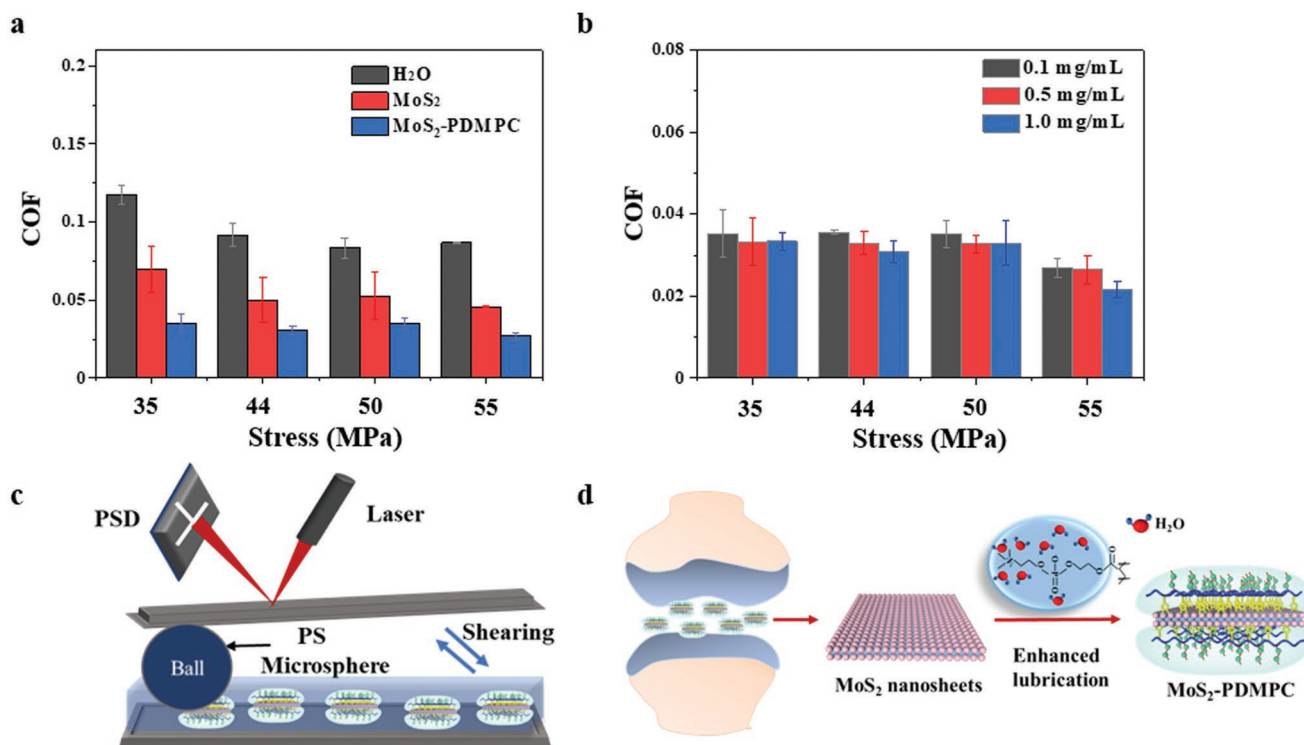
Figure 2. Tribology test for MoS$_2$-PDMPC. a) Lubrication properties of H$_2$O, MoS$_2$, and MoS$_2$-PDMPC at scanning rate of 2 Hz. b) Lubrication properties of different concentrations of MoS$_2$-PDMPC aqueous solution at scanning rate of 2 Hz. c) Schematic diagram of tribology test performed on atomic force microscope (AFM). PSD, position-sensitive detector. PS microsphere, polystyrene microsphere. d) Solid–liquid composite lubrication of MoS$_2$-PDMPC nanosheets.

thermal stability. Excessively high temperature will affect cell activity and cause tissue damage. Therefore, it is very important to select appropriate concentration of MoS$_2$-PDMPC-DS and laser power for the later verification of in vitro and in vivo therapeutic effects. The experimental results show that when the concentration of MoS$_2$-PDMPC-DS is lower than 0.6 mg mL^{-1} and the laser power density is lower than 0.8 W cm^{-2}, the maximum temperature after NIR laser irradiation is lower than 42 °C, which are considered as suitable for later experiments.

2.4. Drug Loading and Release Capacities of MoS$_2$-PDMPC-DS

First, the absorbance of DS at different concentrations were recorded by a UV–vis spectrophotometer (Figure 3f) and the calibration curve of DS was shown in Figure S2 (Supporting Information). The drug loading capacity of MoS$_2$-PDMPC-DS is ≈8.5%. Under NIR laser irradiation, MoS$_2$-PDMPC-DS can undergo photothermal conversion to trigger drug release and exert anti-inflammatory effects. Figure 3g shows that without NIR laser irradiation, only 7.03% DS is released within 1 h. While the release rate of DS is significantly increased by 21.99% under NIR laser irradiation (0.2 W cm^{-2}, 10 min). Without NIR laser irradiation, the drug release rate increases by ≈1%–3% per hour and reaches a maximum release rate of 19.95% after 8 h. However, after repeated NIR laser irradiation (0.2 W cm^{-2}, 10 min) for 8 times, 41.04% DS is released. Meanwhile, the results of drug release experiments show that the drug

release rate of MoS$_2$-PDMPC-DS is positively correlated with the NIR laser power. The higher the power is, the higher the drug release rate. The drug release rate of MoS$_2$-PDMPC-DS (0.2 mg mL^{-1}) reaches 65.98% under NIR laser irradiation (1 W cm^{-2}, 10 min). The excellent and efficient drug release performance of MoS$_2$-PDMPC-DS under NIR laser irradiation is an important prerequisite for the treatment of osteoarthritis. MoS$_2$-PDMPC-DS can smartly release drugs under NIR laser irradiation, which allows us to effectively control the amount and action time of the drug for the treatment of osteoarthritis. Briefly, to treat osteoarthritis, we inject MoS$_2$-PDMPC-DS into the joint cavity and apply an NIR laser in vitro to control drug release.

2.5. Cytotoxicity of MoS$_2$-PDMPC-DS and Macrophage Uptake

Chondrocytes and murine monocyte-macrophage cell line (RAW 264.7) are used for the in vitro experiments. To assess the potential of using MoS$_2$-PDMPC-DS in the treatment of osteoarthritis, we investigate the in vitro cytotoxicity of MoS$_2$-PDMPC-DS on the experimental cells. The results of the Cell Counting Kit-8 (CCK-8) assay (**Figure 4**a,b) show that the survival rate of chondrocytes and RAW264.7 cells is up to 90% when the concentration of MoS$_2$-PDMPC-DS is lower than 200 μg mL^{-1}. The results of live/dead staining (Figure 4c,d) are consistent with the results of CCK-8, which further verifies the biocompatibility of MoS$_2$-PDMPC-DS. MoS$_2$-PDMPC-DS can be interpreted to have good biocompatibility with no obvious cytotoxicity to chondrocytes
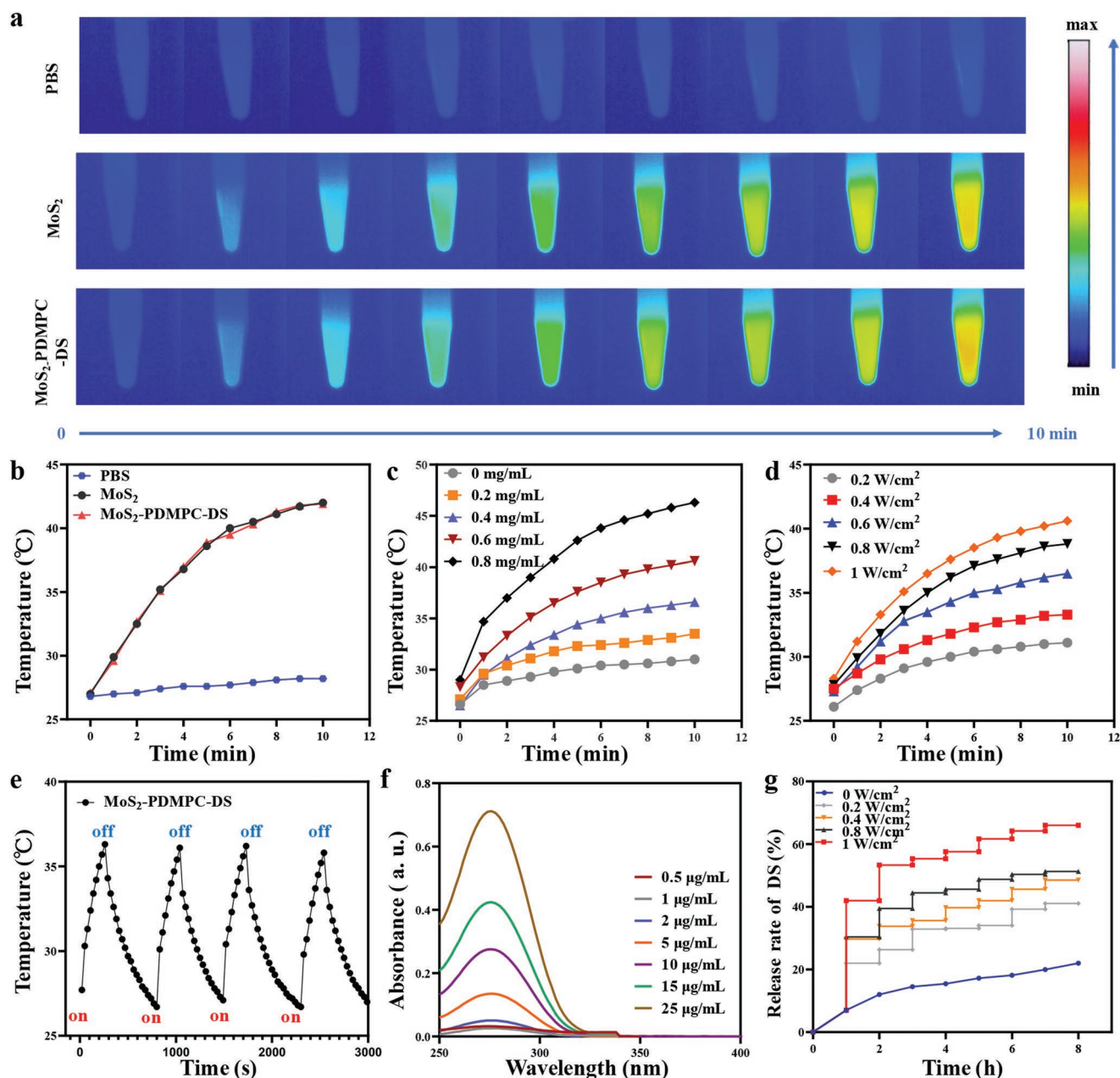
Figure 3. Photothermal conversion property of MoS$_2$-PDMPC-DS and the drug release of MoS$_2$-PDMPC-DS under 808 nm NIR laser irradiation. a) The photothermal images of MoS$_2$ and MoS$_2$-PDMPC-DS under 808 nm NIR laser irradiation (1 W cm^{-2}). b) The temperature changes of MoS$_2$, MoS$_2$-PDMPC, and MoS$_2$-PDMPC-DS (1 mg mL^{-1}) under 808 nm NIR laser irradiation (1 W cm^{-2}). c) The temperature changes of MoS$_2$-PDMPC-DS with different concentrations under 808 nm NIR laser irradiation (1 W cm^{-2}). d) The temperature changes of MoS$_2$-PDMPC-DS (0.6 mg mL^{-1}) under 808 nm NIR laser irradiation at different power densities. e) Thermal stability of MoS$_2$-PDMPC-DS (0.6 mg mL^{-1}) under repeated NIR laser irradiation (1 W cm^{-2}). f) UV–vis spectra of DS at different concentrations. g) Drug release of MoS$_2$-PDMPC-DS (2 mg mL^{-1}) under 808 nm NIR laser irradiation at different power densities.

and macrophages. Since osteoarthritis treatment often requires repeated drug administration, we further examine whether continuous administration of MoS$_2$-PDMPC-DS can be cytotoxic to chondrocytes. CCK-8 and live/dead staining results show that after continuous administration at day 0, 2, 4, and 6 for 24 h, no statistical difference is found between MoS$_2$-PDMPC-DS group and control group, with/without NIR irradiation (Figures S3 and S4, Supporting Information).

The uptake of nanoparticles by the mononuclear phagocytic system (MPS) can affect the retention time of nanoparticles in the MPS, thereby influencing their clearance from the body. To investigate the cellular uptake behavior, we prepared MoS$_2$-PDM@F and MoS$_2$-PDMPC-DS@F by labeling poly (dopamine methacrylamide) (PDM) and PDMPC with fluorescein O-methacrylate (F) and modifying MoS$_2$. Then, the MoS$_2$-PDM@F and MoS$_2$-PDMPC-DS@F were cocultured with
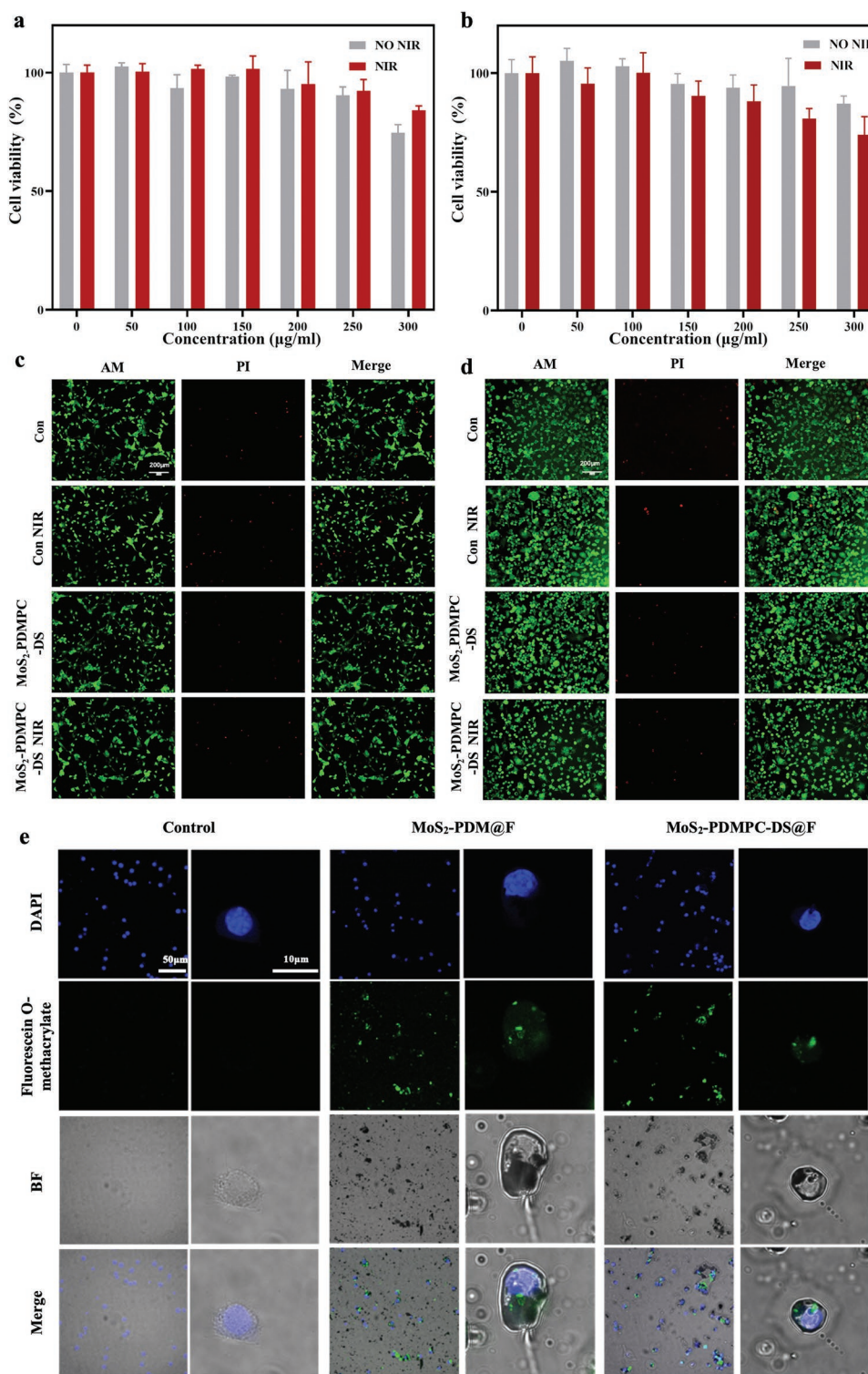
Figure 4. Cytotoxicity and cellular uptake of MoS$_2$-PDMPC-DS. a) The effect of MoS$_2$-PDMPC-DS on the cell viability of macrophages with or without NIR laser irradiation detected by CCK-8. b) The effect of MoS$_2$-PDMPC-DS on the cell viability of chondrocytes with or without NIR laser irradiation detected by CCK-8. c) Live/dead fluorescence images of macrophages cultured with MoS$_2$-PDMPC-DS for 24 h with or without NIR laser irradiation. AM, calcein-acetoxymethyl. PI, propidium iodide. d) Live/dead fluorescence images of chondrocytes cultured with MoS$_2$-PDMPC-DS for 24 h with or without NIR laser irradiation. e) Uptake of the MoS$_2$-PDM@F and MoS$_2$-PDMPC-DS@F by macrophages after incubation for 4 h. DAPI, 2-(4-amidinophenyl)-6-indolecarbamidine dihydrochloride. BF, bright field.

ADVANCED
SCIENCE NEWS
www.advancedsciencenews.com

ADVANCED
FUNCTIONAL
MATERIALS
www.afm-journal.de

macrophages. After incubation for 4 h, MoS$_2$-PDMPC-DS@F group shows significantly fewer intracellular green fluorescence than MoS$_2$-PDM@F group (Figure 4e). Flowcytometry is further performed to verify the macrophage uptake of MoS$_2$-PDM@F and MoS$_2$-PDMPC-DS@F. The result indicates that the uptake ratio of MoS$_2$ (88.2%) is significantly higher than that of MoS$_2$-PDMPC-DS (19.9%) (Figure S5, Supporting Information). To further examine whether mechanisms other than cellular uptake exist, we tested the effect of MoS$_2$-PDMPC-DS on the apoptosis and polarization of lipopolysaccharide (LPS) -activated macrophages by flow cytometry. The results are shown in Figures S6 and S7 (Supporting Information). Compared with LPS activation, MoS$_2$-PDMPC-DS did not show the effect of promoting the apoptosis of macrophages, or obvious effect of promoting the anti-inflammatory M2-type polarization of macrophages. The above results may be related to the fact that DS, which is loaded on MoS$_2$-PDMPC is an NSAID. NSAIDs can reduce the synthesis of prostaglandin E2 (PGE2) by selectively inhibiting COX-2 activity. According to previous literature reports, PGE2 can promote the apoptosis of macrophages and promote M2-type polarization of macrophages.[44–46] In this study, although MoS$_2$-PDMPC-DS doesn't achieve its anti-inflammatory effect by regulating the apoptosis or polarization of macrophages, it can inhibit the intraarticular drug loss effectively through a drastic reduction of macrophage uptake (Figure 4e; Figure S5, Supporting Information). On one hand, effective delivery of anti-inflammatory drugs through photo-controlled release is achieved, which significantly reduces the expression of various inflammatory factors. On the other hand, the wear of articular cartilage can be alleviated by continuous lubrication, which may further reduce the vicious cycle of inflammation and cartilage destruction. Therefore, within the scope of this study, the mechanism of inhibiting macrophage uptake is of great significance for MoS$_2$-PDMPC-DS in reducing osteoarthritis inflammation.

## 2.6. In Vitro Anti-Inflammatory Effect of MoS$_2$-PDMPC-DS

Macrophages, which exist mainly in the synovium of joints, are important components involved in the progression of osteoarthritis. Macrophages can proliferate rapidly in pathological environments and release inflammatory factors, resulting in edema of vascular dilatation tissue and cartilage destruction.[47] LPS can activate macrophages to produce many inflammatory factors (such as tumor necrosis factor alpha (TNF-α), interleukin 1 beta (IL-1β), and interleukin 6 (IL-6)). DS is a kind of NSAID that can inhibit the production of inflammatory factors primarily by inhibiting COX-2 activity. Therefore, both DS and MoS$_2$-PDMPC-DS can limit the production of inflammatory factors by macrophages with or without NIR laser irradiation. As shown in **Figure 5**a–c, LPS activates macrophages to produce TNF-α, IL-1β, and IL-6. Compared with the PBS group, the MoS$_2$-PDMPC-DS group and DS group show reduced production of TNF-α, IL-1β, and IL-6. Without the irradiation of NIR laser, MoS$_2$-PDMPC-DS can slowly release a small dose of DS, and its anti-inflammatory effect is better than the anti-inflammatory effect of the DS group. Under NIR laser irradiation, the MoS$_2$-PDMPC-DS group can sustainedly release

drugs and significantly inhibit the activation of macrophages, reducing the production of TNF-α, IL-1β and IL-6. The anti-inflammatory effect of the MoS$_2$-PDMPC-DS group with NIR laser irradiation is significantly better than that of the other groups. The experimental results verify that MoS$_2$-PDMPC-DS can effectively inhibit the production of inflammatory factors by activated macrophages under NIR laser irradiation, thus regulating the osteoarthritic environment.

However, in the pathological progression of osteoarthritis, a variety of inflammatory mediators and reactive oxygen species (ROS) participate in the degradation of the cartilage matrix. Oxygen free radicals can stimulate the production of inflammatory cytokines and induce cartilage degradation.[48] Collagen type II alpha (Col2α) is one of the major components of the cartilage matrix. When cartilage is in an inflammatory environment, its expression in cartilage is abnormally decreased, and the expression of related proteases such as matrix metalloproteinase 1 (MMP1) is abnormally increased.[49,50] Moreover, tachykinin-1 (TAC1) gene, which is highly related with pain caused by inflammation, can be abnormally increased under inflammatory environment. Hydrogen peroxide (H$_2$O$_2$) is further used to co-culture with chondrocytes in order to create an inflammatory microenvironment.[21] The quantitative real-time polymerase chain reaction (qRT-PCR) results in Figure 5d–f show that H$_2$O$_2$ can decrease the messenger ribonucleic acid (mRNA) expression levels of Col2α and increase the mRNA expression levels of MMP1 as well as TAC1 in chondrocytes. Figure 5d shows that the MoS$_2$-PDMPC-DS group without NIR laser irradiation and the DS group have a reversal effect on the mRNA expression of Col2α in chondrocytes co-incubated with H$_2$O$_2$, but the effect is not as obvious as that of MoS$_2$-PDMPC-DS with NIR laser irradiation. MoS$_2$-PDMPC-DS with NIR laser irradiation effectively reverses the mRNA expression level of Col2α in the chondrocytes co-incubated with H$_2$O$_2$, reaching 75.09% of that in the control group (normal chondrocytes). Figure 5e,f shows that the MoS$_2$-PDMPC-DS and DS have an effect on reducing the mRNA expression levels of MMP1 and TAC1 in chondrocytes co-incubated with H$_2$O$_2$. Among these groups, MoS$_2$-PDMPC-DS with NIR laser irradiation effectively reduces the mRNA expression levels of MMP1 and TAC1 in H$_2$O$_2$ co-incubated chondrocytes.

In addition, to further verify the effect of MoS$_2$-PDMPC-DS on chondrocytes, immunofluorescence staining is used to detect the expression of Col2α in chondrocytes. Normal chondrocytes are set as the control group, and chondrocytes co-cultured with H$_2$O$_2$ without any treatment are set as the PBS group. As shown in Figure 5g, the expression level of Col2α in chondrocytes co-cultured with H$_2$O$_2$ is significantly decreased, and the fluorescence intensity in the PBS group is fully weak. The MoS$_2$-PDMPC-DS group without NIR laser irradiation and the DS group improve the Col2α protein expression level in chondrocytes co-incubated with H$_2$O$_2$. However, they are not as effective as MoS$_2$-PDMPC-DS with NIR laser irradiation, and the experimental results show that MoS$_2$-PDMPC-DS can effectively improve the Col2α expression level of chondrocytes co-incubated with H$_2$O$_2$ with NIR laser irradiation. The above results indicate that under NIR laser irradiation, MoS$_2$-PDMPC-DS can regulate the expression of Col2α, MMP1, and TAC1 to alleviate cartilage damage and pain under oxidative stress. As the
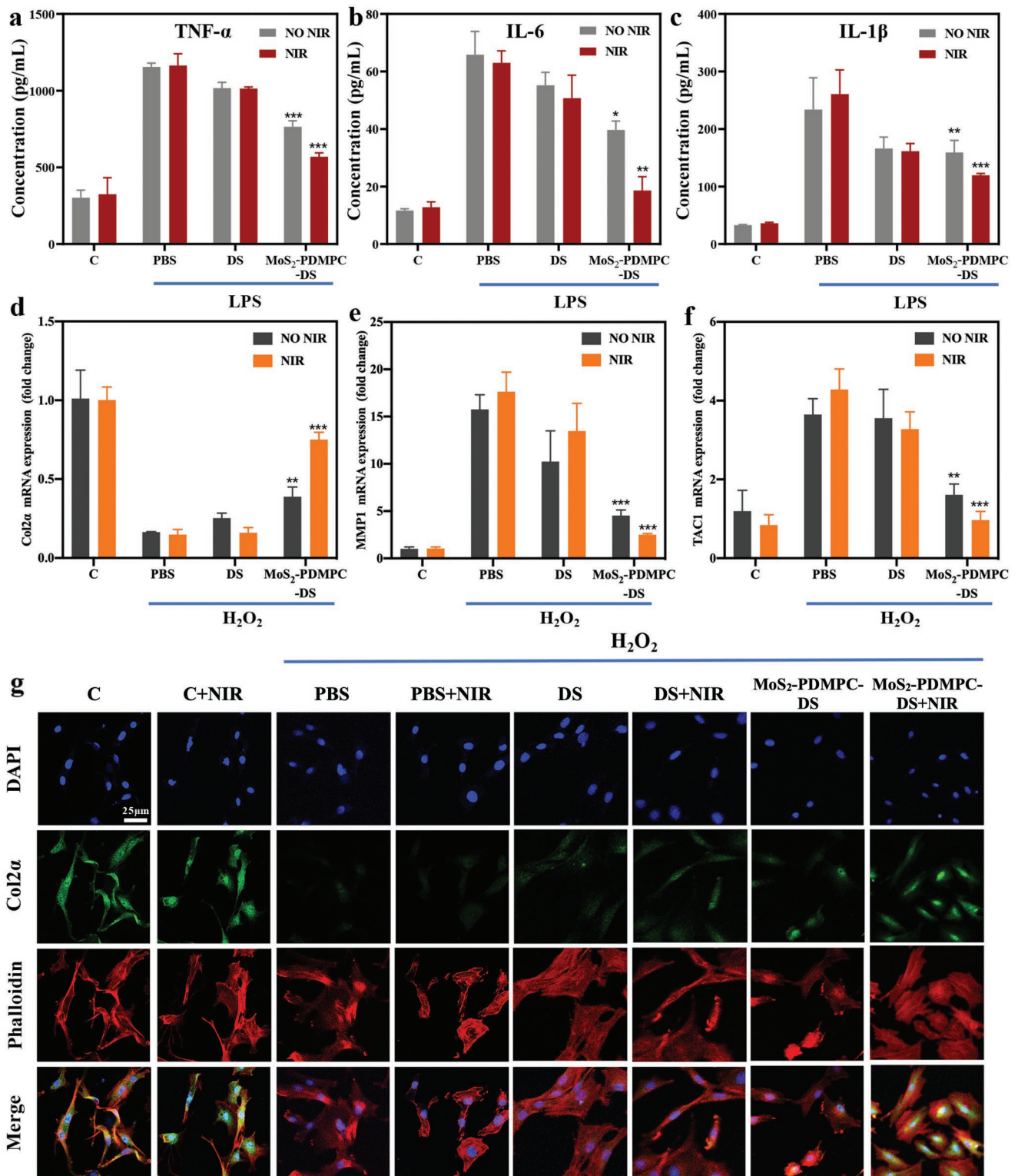
Figure 5. Anti-inflammation mechanism of MoS₂-PDMPC-DS on macrophages and chondrocytes. a–c) Enzyme-linked immunosorbent assay (ELISA) results for the protein expression levels of TNF-α, IL-6, and IL-1β after LPS activation of RAW 264.7 macrophages co-incubated with DS and MoS₂-PDMPC-DS for 24 h with or without NIR laser irradiation ($n = 3$, each data point is shown as mean ± standard deviation (SD), $*p < 0.05$, $**p < 0.01$, $***p < 0.001$, compared with the PBS group). d–f) qRT-PCR analysis for the mRNA expression levels of Col2α, MMP1 and TAC1 of chondrocytes, which are co-incubated with H₂O₂ for 24 h and then cultured with DS or MoS₂-PDMPC-DS for 24 h with or without NIR laser irradiation ($n = 3$, each data point is shown as mean ± SD, $*p < 0.05$, $**p < 0.01$, $***p < 0.001$, compared with the PBS group). g) Representative fluorescence images showing the expression of Col2α in chondrocytes co-incubated with DS and MoS₂-PDMPC-DS for 24 h with or without NIR laser irradiation after H₂O₂ stimulation.

ADVANCED
SCIENCE NEWS

www.advancedsciencenews.com

ADVANCED
FUNCTIONAL
MATERIALS

www.afm-journal.de

lubrication effect of PDMPC cannot be investigated in the in vitro experiments, MoS_2-PDMPC-DS mainly releases DS to inhibit the activation of macrophages and regulate oxidative stress to alleviate osteoarthritis inflammation. The NIR laser irradiation can effectively improve drug release rate and utilization, endowing MoS_2-PDMPC-DS with an excellent anti-inflammatory effect. Meanwhile, the above experiments prove that the effects of the control group, PBS group, and DS group are not significantly different with or without NIR laser irradiation.
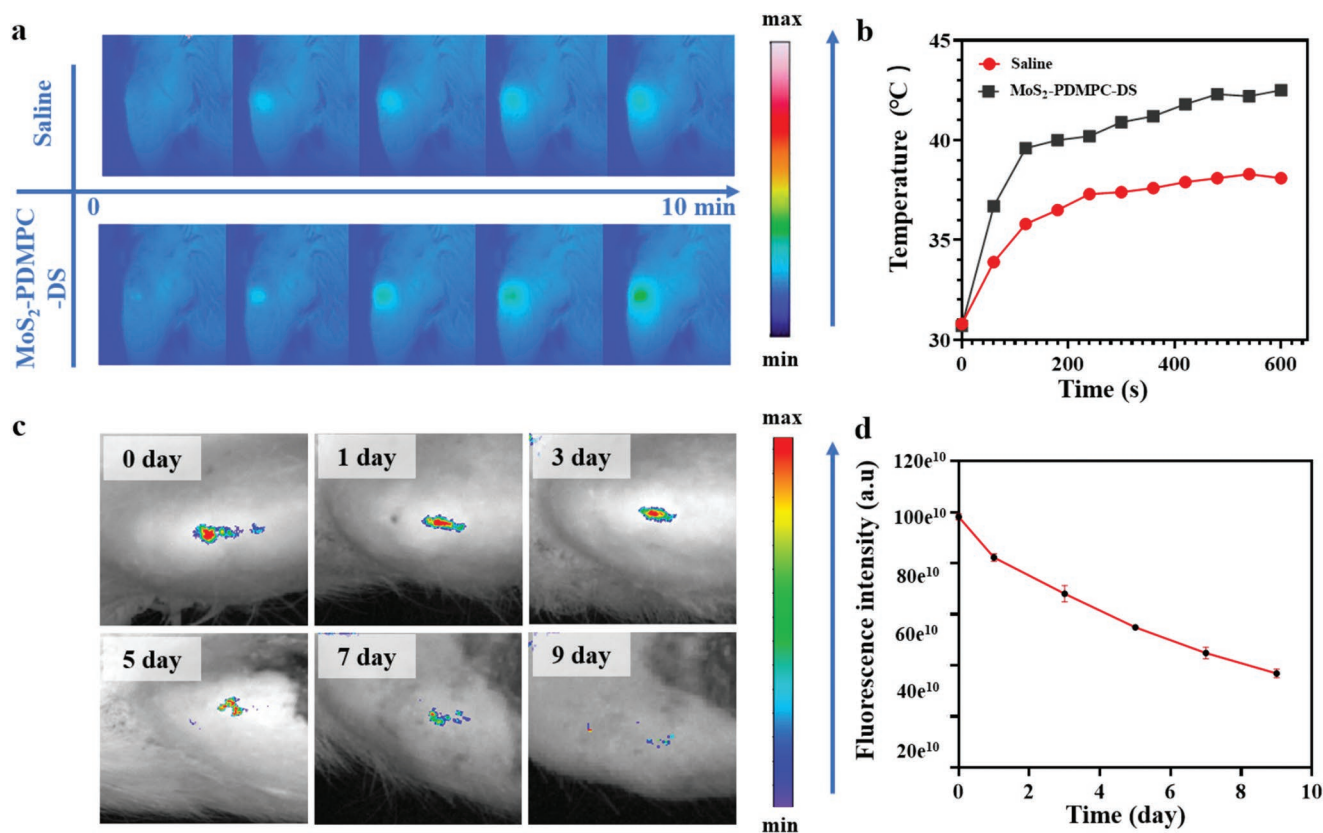
2.7. Photothermal Effect and Retention of MoS_2-PDMPC-DS in Rat Joint Cavity

The retention time and photothermal conversion efficiency of MoS_2-PDMPC-DS in the articular cavity determine its therapeutic effect on osteoarthritis. To investigate whether MoS_2-PDMPC-DS responds to the NIR laser in the joint cavity of rats, photothermal images of rat joints after injection with MoS_2-PDMPC-DS or saline under NIR laser irradiation are obtained by a near-infrared camera. **Figure 6**a,b shows that the temperature in the joint cavity of rats injected with MoS_2-PDMPC-DS increases significantly under NIR laser irradiation and reached 43.2 °C in 10 min. The temperature in the joint cavity of rats injected with saline remains at 37 °C. The NIR laser

has good tissue penetration and low tissue absorption,[51] therefore the NIR laser can be used as a smart response switch of MoS_2-PDMPC-DS. The temperature change of MoS_2-PDMPC-DS in the joint cavity confirms this assumption, which is one of the prerequisites of MoS_2-PDMPC-DS as a photo-responsive drug-release system for the treatment of osteoarthritis.

To evaluate the retention time of MoS_2-PDMPC in the joint cavity, MoS_2-PDMPC-DS@F is injected into the knee joint cavity of rats, and a small animal fluorescence imaging system is used to observe the retention of MoS_2-PDMPC in the joint cavity at 0, 1, 3, 5, 7, and 9 days. The results show that the fluorescence intensity gradually decreases following injection of the material. On day 5, the fluorescence intensity still retains 56.0% of the initial value, and on day 9, the fluorescence intensity drops to 37.5% (Figure 6c,d). However, after intra-articular injection of MoS_2-PDM@F, the fluorescence intensity drops to 38.5% at day 5 (Figures S8 and S9, Supporting Information). These results further prove that MoS_2-PDMPC can stay in the joint cavity longer than MoS_2-PDM. Combined with the previous in vitro macrophage uptake assays, it can be inferred that the formation of hydration layer and the inhibited uptake of macrophages due to PDMPC modification might be a reason for the prolonged retention of MoS_2-PDMPC in joint cavity.

The morphology of MoS_2-PDMPC-DS after dispersed in simulated physiological liquids are observed using scanning electron

Figure 6. Photothermal conversion properties and retention of MoS_2-PDMPC-DS in the articular cavity of rats. a) Photothermal image of the rat's articular cavity after injecting MoS_2-PDMPC-DS or saline with NIR laser irradiation (the power density of NIR laser is 0.6 W cm^{-2}). b) Temperature changes of the rat's articular cavity after injecting MoS_2-PDMPC-DS or saline with NIR laser irradiation. c) Fluorescence imaging of articular cavity in rats after injecting MoS_2-PDMPC at 0, 1, 3, 5, 7, and 9 days, respectively. d) Fluorescence intensity of articular cavity in rats after the injection of MoS_2-PDMPC at 0, 1, 3, 5, 7, and 9 days, respectively.

microscope (SEM). As Figure S10 (Supporting Information) shows, after incubation in PBS/fetal bovine serum (FBS) for one week, MoS$_2$-PDMPC-DS still maintains layered structure the same as the original, which further proves the stability of MoS$_2$-PDMPC-DS in physiological environment.

2.8. Therapeutic Effect of MoS$_2$-PDMPC-DS on a Rat Osteoarthritis Model

A rat osteoarthritis model is successfully established by anterior cruciate ligament transection (ACLT) and meniscectomy. To evaluate the therapeutic effect of MoS$_2$-PDMPC-DS on rat osteoarthritis, we perform radiological and histological analyses of the knee joints of different groups. In the early stage of osteoarthritis, the main manifestations are vascular expansion and joint tissue edema. With the aggravation of inflammation, the cartilage surface is further worn and cartilage is destroyed and degenerated, resulting in calcification and the formation of osteophytes with uneven density and irregular shape. X-ray is used to analyze the bone morphology and cone beam computed

tomography (CBCT) is used to measure the knee joint space in each group after 2/4 weeks of intervention. At 2 weeks, the bone density of knee joint in the osteoarthritis (OA), DS, and MoS$_2$-PDMPC-DS groups is decreased, indicating that bone is destroyed and the articular surface is blurred. Among these groups, the OA group has the most severe bone destruction. The MoS$_2$-PDMPC-DS with NIR laser group shows less bone destruction and the best therapeutic effect, which is close to the control group (**Figure 7**a). After four weeks of intervention, except for the control group, the damage degree of joint in the other groups increases. Among these groups, the knee joint in the OA group has the highest degree of joint lesions. Compared with the DS group, the joint damage in the MoS$_2$-PDMPC-DS without NIR laser group is less severe. The joint aggravation and damage in the MoS$_2$-PDMPC-DS with NIR laser group are the mildest due to the solid–liquid composite lubrication of MoS$_2$-PDMPC-DS and the efficient release of DS under NIR laser irradiation (Figure 7b). The formation of osteophytes in osteoarthritis can cause joint space to become blurred. The measured joint space based on CBCT images shows that the joint space of the OA group is narrower than that of the DS
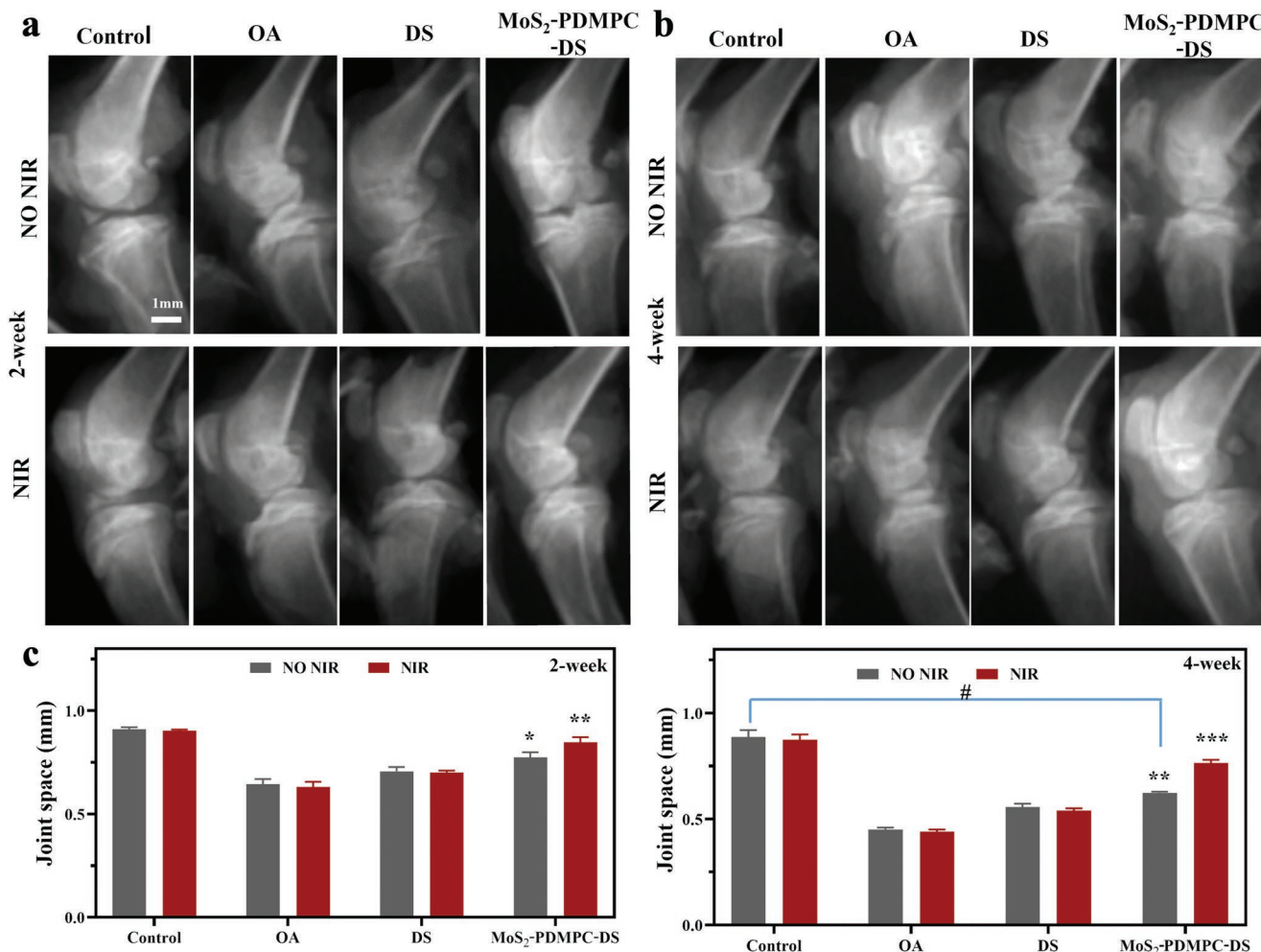
Figure 7. Radiography of knee joint in rats. a,b) Representative X-ray examination of rats after 2 and 4 weeks of the intervention (the power density of NIR laser is 0.6 W cm^{-2}). c) Joint space of rats after 2 and 4 weeks of the intervention measured based on the CBCT images ($n = 3$, each data point is shown as mean ± SD, *$p < 0.05$, **$p < 0.01$, ***$p < 0.001$, compared with the OA group. #$p < 0.05$, compared with the control group). OA, osteoarthritis.

**ADVANCED
SCIENCE NEWS**
www.advancedsciencenews.com

**ADVANCED
FUNCTIONAL
MATERIALS**
www.afm-journal.de

group and the MoS_2-PDMPC-DS group after intervention. At 4 weeks of intervention, the joint space decreases in all groups except the control group compared with the results at 2 weeks. The joint space of the MoS_2-PDMPC-DS group is significantly larger than that of the OA group and DS group with or without NIR irradiation, indicating that the long-term efficacy of synergetic lubrication and anti-inflammation is better than that of using anti-inflammatory treatment alone. Notably, at 4 weeks, the joint space of the MoS_2-PDMPC-DS group without NIR irradiation is significantly different from the joint space of the

control group ($p < 0.05$), but there is no significant difference between the MoS_2-PDMPC-DS group with NIR irradiation and the control group ($p > 0.05$), indicating that the synergistic treatment of enhanced lubrication and photo-controlled release of anti-inflammatory agents has a better therapeutic effect than just using lubrication and sustained release of anti-inflammatory agents. (Figure 7c). To illustrate the progress of knee osteoarthritis more clearly in different groups, the micro-CT images of the knee joint in each group are detected at 2 and 4 weeks after intervention (**Figure 8**a,b). The area of bone destruction
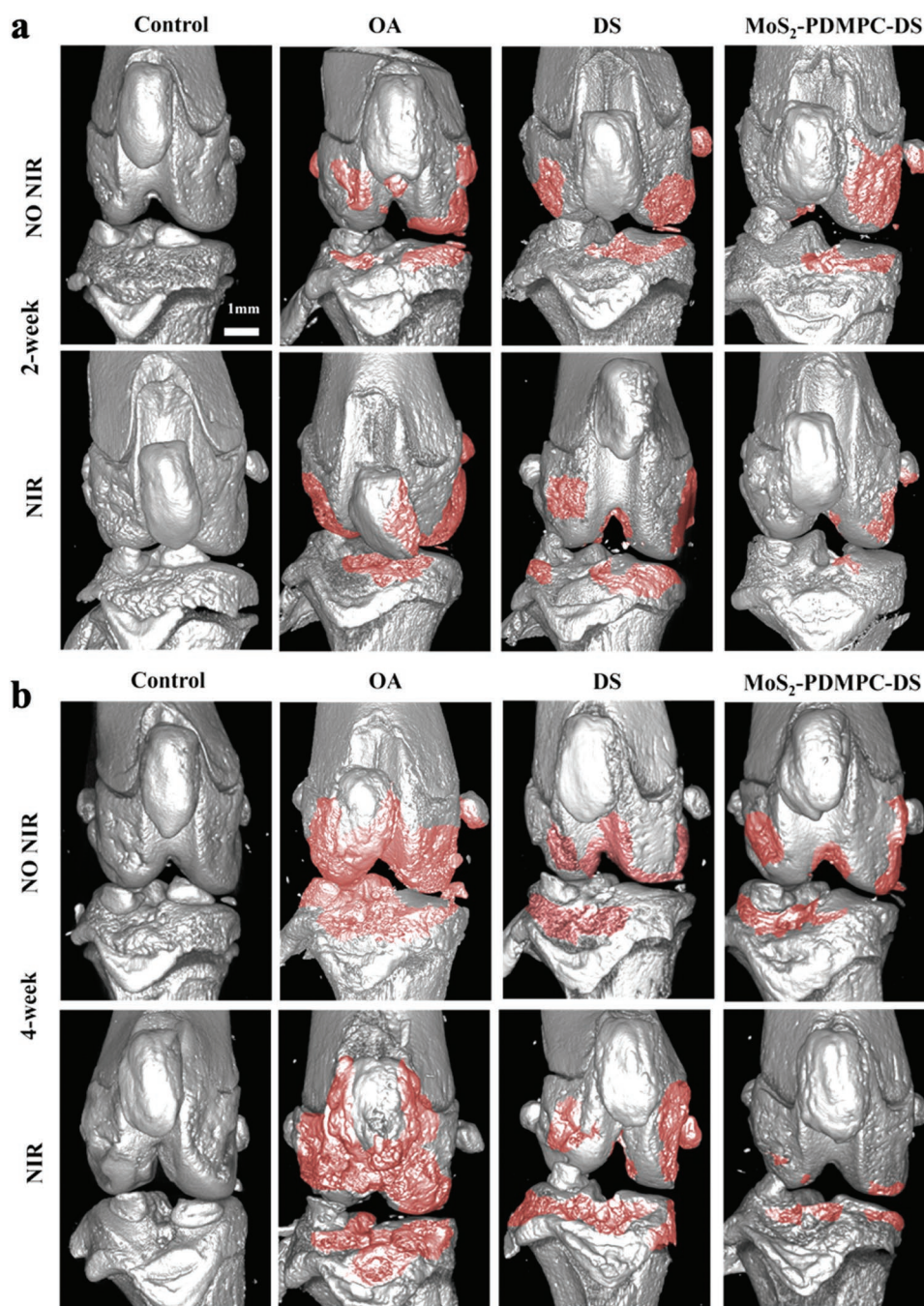
Figure 8. Micro-CT images of the knee joints for the rats in control, OA, DS, and MoS_2-PDMPC-DS groups with or without NIR laser irradiation at a) 2-week and b) 4-week. The power density of NIR laser is 0.6 W cm^{-2}.

and osteophyte formation (red part) in MoS$_2$-PDMPC-DS with the NIR laser group is significantly less than that of other groups. The results are consistent with the X-ray images, which prove that MoS$_2$-PDMPC-DS can effectively treat osteoarthritis and alleviate the deterioration of osteoarthritis.

To further clarify the therapeutic effect of MoS$_2$-PDMPC-DS on osteoarthritis, the knee joints of the rats after 4 weeks of intervention are stained with hematoxylin and eosin (HE) and Safranin O-fast green, and histopathological scoring is performed in different groups. The main pathological changes of osteoarthritis are cartilage fissure, chondrocyte degeneration and necrosis, and osteophyte formation. The HE staining results (**Figure 9**a) show that the articular cartilage in the control group is smooth and continuous, and the chondrocytes are regularly and tightly arranged, while the articular cartilage in the OA, DS, and MoS$_2$-PDMPC-DS groups is rough and cracked. Cartilage degeneration and destruction are the most obvious in the OA group, followed by the DS group and the MoS$_2$-PDMPC-DS group without NIR laser irradiation. The cartilage destruction in the MoS$_2$-PDMPC-DS group with NIR laser irradiation is the lowest. The cartilage is stained red by safranin O-fast. Safranin O binds to polyanionic substances in proteoglycans in a positive proportion, which indirectly reflects the content and distribution of glycosaminoglycan in the matrix. When cartilage is damaged, glycoprotein components in cartilage will be released, and matrix components will be unevenly distributed, resulting in less or no safranin staining. Figure 9b shows that the cartilage coloration in the OA group is shallow and uneven, while the control group shows that the cartilaginous safranine O is clearly colored and evenly distributed. In all treatment groups, the depth of cartilage staining shows a trend of MoS$_2$-PDMPC-DS group > DS group > OA group, indicating that anti-inflammatory treatment alone alleviates the loss of proteoglycan caused by cartilage destruction in osteoarthritis to a certain extent, and the synergistic treatment of anti-inflammation and lubrication is better than the single anti-inflammatory treatment. Among these treatments, the cartilage staining depth of the MoS$_2$-PDMPC-DS group with NIR laser irradiation is deeper than the cartilage staining depth of the MoS$_2$-PDMPC-DS without NIR laser group, indicating that on the basis of lubrication treatment, the effect of photo-controlled release of anti-inflammatory drug was better than the effect of simple sustained release. The glycosaminoglycan (GAG) content in the cartilage of each group is further quantitatively analyzed. It is found that the GAG contents of the OA group and DS group are 25.3% and 36.9% of that of the control group, and there is no significant difference between the OA group and the DS group. Combined with the results of HE staining, this phenomenon indicates that although anti-inflammatory treatment can improve the continuity of the cartilage surface to a certain extent, its ability to alleviate the loss of GAG is limited. The GAG contents of the MoS$_2$-PDMPC-DS group without NIR laser irradiation and the MoS$_2$-PDMPC-DS group with NIR laser irradiation are 52.4% and 70.1% of the GAG content of the control group, respectively, which are significantly higher than the GAG content of the OA group (Figure 9c). The MoS$_2$-PDMPC-DS group with NIR laser irradiation shows the best treatment effect. Osteoarthritis Research Society International (OARSI) scoring is performed for each group based on the degree of cartilage damage. Compared with the OA group, the OARSI value of the MoS$_2$-PDMPC-DS with NIR laser irradiation decreases significantly (Figure 9d). The above results further confirm the excellent therapeutic effect of MoS$_2$-PDMPC-DS with NIR laser irradiation.

Col2α protein is a major biomarker of articular cartilage. The expression of Col2α in normal cartilage tissue is evenly distributed. Immunohistochemical staining is used to detect the expression of Col2α protein in cartilage tissue and can reflect the pathological state of articular cartilage in different groups. **Figure 10**a,b shows that Col2α protein expression in the control group is uniform and obvious, but almost no expression is observed in the OA group. The expression of Col2α protein in the MoS$_2$-PDMPC-DS group is higher than that of the DS group. The expression of Col2α protein in the MoS$_2$-PDMPC-DS with NIR laser irradiation group is most obvious because MoS$_2$-PDMPC-DS has the function of solid–liquid synergistic lubrication and can release DS to produce anti-inflammatory effects, especially with NIR laser irradiation. Therefore, the intra-articular injection of MoS$_2$-PDMPC-DS can effectively lubricate joints and delay the progression of osteoarthritis. Due to the short half-life of DS, the drug will be rapidly metabolized after being injected into the joint cavity,[52] therefore the intra-articular injection of DS has relatively limited effect on the alleviation of osteoarthritis. MoS$_2$-PDMPC-DS can prolong the retention time of DS in the joint cavity and effectively release DS under NIR laser irradiation to regulate the action time of anti-inflammatory drugs. In addition, MoS$_2$-PDMPC-DS has solid–liquid composite lubrication properties, which can achieve the effect of anti-inflammatory and lubricating synergistic treatment of osteoarthritis. The results of imaging and histological experiments show that MoS$_2$-PDMPC-DS can effectively relieve the progression of osteoarthritis under NIR laser irradiation. Therefore, it can potentially be used as a method for osteoarthritis injection therapy to improve the therapeutic effect and relieve the pain of patients.

2.9. In Vivo Biosafety

To evaluate the in vivo biosafety of MoS$_2$-PDMPC-DS, the HE-stained sections of the major organs, such as the heart, liver, spleen, lung, and kidney, in rats after 4 weeks of intervention are analyzed. The staining results are shown in Figure S11 (Supporting Information). There are no pathological changes, such as degeneration, necrosis, or edema, in the five internal organs of the rats in each group. The tissue texture of each organ is clear, and the cells are arranged in a tight and orderly manner. Therefore, it is considered that the long-term presence of MoS$_2$-PDMPC-DS in the joint cavity will not cause toxicity or side effects to the body.

3. Conclusions

In this study, we applied the concept of solid–liquid composite lubrication to the treatment of osteoarthritis and successfully synthesized a photo-responsive biomimetic 'nano-snowboard', MoS$_2$-PDMPC-DS, that could sustainably exert dual-functions
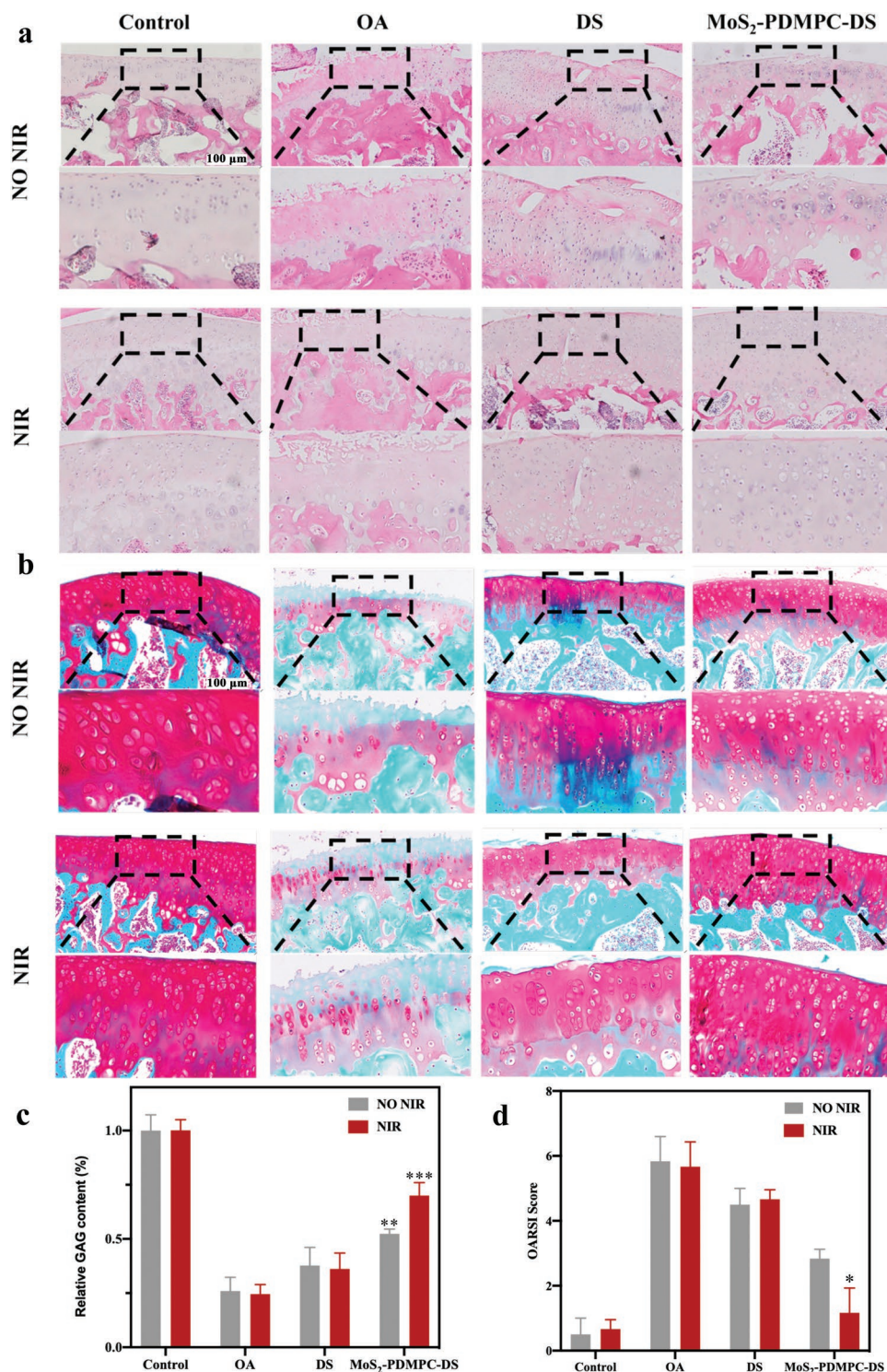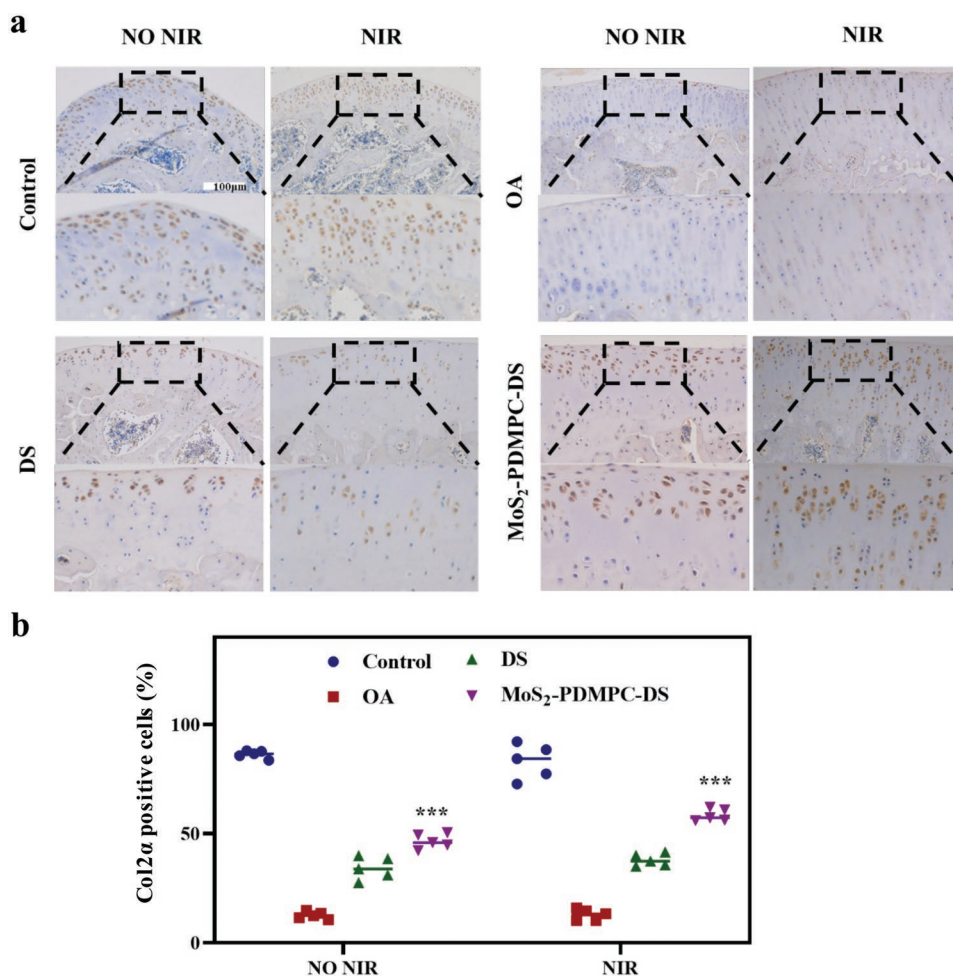
Figure 9. Histological analysis of knee joint tissue. a) HE staining and b) Safranin O-fast green staining of knee joint tissue for the control, OA, DS, and MoS$_2$-PDMPC-DS groups with or without NIR laser irradiation after 4 weeks of intervention. Scale bar: 100 μm. c) Relative GAG content and d) OARSI score of the control, OA, DS, and MoS$_2$-PDMPC-DS groups after 4 weeks of intervention ($n = 3$, each data point is shown as mean ± SD, *$p < 0.05$, **$p < 0.01$, ***$p < 0.001$, compared with the OA group).

of anti-inflammation and lubrication. The biomimetic polymer of PDMPC with lubrication properties was modified on MoS$_2$ nanosheets and formed a hydration layer on the surface, which improved the stability of the nanosheets and endowed the nanosheets with dual properties of solid-phase and liquid-phase lubrication. Additionally, DS was loaded on the nanosheets to

**ADVANCED
SCIENCE NEWS**

www.advancedsciencenews.com

**ADVANCED
FUNCTIONAL
MATERIALS**

www.afm-journal.de

Figure 10. Immunohistochemical evaluation of knee joint tissue. a) Immunohistochemical staining of Col2α for each group after 4 weeks of intervention. b) The quantitative data of Col2α positive cells (n = 5, each data point is shown as mean ± SD, ***p < 0.001, compared with the OA group).

exert a high-efficiency and anti-inflammatory effect under NIR laser irradiation. The in vitro and in vivo experiments demonstrated that the lubrication properties of MoS$_2$ nanosheets modified with PDMPC were significantly improved and remained stable in the joint cavity for more than one week. The drug release experiments proved that the NIR laser irradiation could efficiently promote the release of drugs from MoS$_2$-PDMPC-DS nanosheets. The cell and animal experiments showed that MoS$_2$-PDMPC-DS could effectively reduce the production of inflammatory factors such as TNF-α, IL-6, and IL-1β, alleviate cartilage wear and reduce the formation of osteophytes, and thus achieving effective treatment for rat osteoarthritis. As a novel photoresponsive solid–liquid composite lubrication 'nano-snowboard', MoS$_2$-PDMPC-DS was the first to achieve excellent therapeutic effect on osteoarthritis. In addition, MoS$_2$-PDMPC-DS also had the characteristics of remotely controlled drug release, long-term stability, and efficient anti-inflammatory activity. Consequently, MoS$_2$-PDMPC-DS has excellent application potential in the treatment of osteoarthritis and can be used as an intra-articular injection material to effectively treat osteoarthritis.

4. Experimental Section

Materials: MoS$_2$ powder, *N*-methylpyrrolidone, *N*,*N*-dimethylformamide (DMF), *N*-methylpyrrolidone, and 2,2'-azobis(2-methylpropionitrile) (AIBN) were purchased from Sinopharm Chemical Reagent Co., Ltd. (Beijing, China). DS, collagenase II, and CCK-8 were purchased from Solarbio Science & Technology Co., Ltd. (Beijing, China). Live/Dead Cell Staining Kit, Dulbecco's modified Eagle's medium (DMEM), FBS, and 1% antibiotics were purchased from Thermo Fisher Scientific (Gibco, Grand Island, NY, USA). LPS, paraformaldehyde, TritonX-100, anti-Col2α monoclonal antibody, fluorescent conjugated secondary antibody, DAPI, and TRIzol reagent were purchased from Sigma–Aldrich (Shanghai, China). ELISA kits were purchased from Beijing 4 A Biotech Co., Ltd. Reverse transcription system Kit and SYBR Premix Ex Tag Kit were purchased from Takara Bio Inc. (Shanghai, China).

Synthesis of MoS$_2$-PDMPC-DS: MoS$_2$ nanosheets were prepared by a liquid exfoliation process. MoS$_2$ powder (100 mg) was added to 30 mL *N*-methylpyrrolidone and then sonicated for 24 h in an ultrasonic bath at 20 °C. The black suspension obtained was centrifuged at 2000 rpm for 20 min to remove large or thick MoS$_2$ nanosheets. Finally, ultrathin MoS$_2$ nanosheets were extracted by high-speed centrifugation (12000 rpm, 30 min). Afterward, the underlayer precipitate was washed with deionized water and ethanol to obtain MoS$_2$ nanosheets. The copolymer PDMPC containing dopamine methacrylamide (DMA)

and 2-methacryloyloxyethyl phosphorylcholine (MPC) was synthesized according to the previous study.[53] Briefly, DMA (4 mM) and MPC (4 mM) were dissolved in 90 mL DMF, and AIBN (0.02 mM) was added to the mixture as an initiator. Then, the reaction mixture was heated to 70 °C for 14 h under a nitrogen atmosphere. The copolymer PDMPC was obtained by dialysis against deionized water and freeze-drying. MoS$_2$ nanosheets (100 mg) and PDMPC (1 g) were evenly dispersed in 10 mL Tris-HCl buffer (pH 8.5, 0.5 M) and then sonicated for 24 h in an ultrasonic bath at 20 °C. The PDMPC-modified MoS$_2$ nanosheets (MoS$_2$-PDMPC) were collected by high-speed centrifugation (12000 rpm, 30 min) and a freeze-drying process. For the preparation of MoS$_2$-PDMPC-DS, 100 mg of MoS$_2$ nanosheets, 1 g of PDMPC and 20 mg of DS were uniformly dispersed in 10 mL Tris-HCl buffer (pH 8.5, 0.5 M) and magnetically stirred at 25 °C for 24 h. Then, the mixture was centrifuged (12000 rpm, 30 min), repeatedly washed with PBS to remove unloaded DS, and freeze-dried overnight to obtain MoS$_2$-PDMPC-DS.

Characterization of MoS$_2$ Nanosheets and MoS$_2$-PDMPC-DS: The surface morphology and crystallographic structure of MoS$_2$ nanosheets were determined using TEM (H-7650B, Hitachi, Japan), HRTEM (JEM-2100F, JEOL, Japan), and SAED imaging. Elemental analysis of MoS$_2$ was captured by HRTEM and energy-dispersive X-ray spectroscopy (EDX). The particle size and zeta potential of MoS$_2$, MoS$_2$-PDMPC, and MoS$_2$-PDMPC-DS were measured by a Nano ZS size analyzer (ZS90, Malvern, UK). FTIR spectroscopy spectra of DS, PDMPC, MoS$_2$-PDMPC, and MoS$_2$-PDMPC-DS at the wavenumber ranging from 500 to 4000 cm^{-1} were recorded by an FTIR spectrometer (Nicolet 6700, Thermo Scientific, USA). The UV absorption spectra of MoS$_2$, DS, PDMPC, MoS$_2$-PDMPC, and MoS$_2$-PDMPC-DS were measured by a Metash UV-6100A spectrometer (Shanghai, China). The X-ray diffraction (XRD) spectrum of MoS$_2$ was recorded on a Bruker AXS D8 Diffractometer (Bruker, Germany) with a 2θ range from 0.6 to 10°. The layered structure and vibration frequency of the nanosheets were detected by XploRA Plus Raman spectrometer (Horiba, France).

Lubrication Test: A series of tribological tests were carried out to investigate the lubrication properties of MoS$_2$ nanosheets with or without PDMPC using an AFM (MFP-3D, Asylum Research). The AFM experiments were performed in a contact mode between a silicon wafer substrate and a rectangular tipless cantilever (TL-CONT) attached with a PS microsphere (diameter: 5 μm). The PS microsphere was glued to a rectangular tipless cantilever by UV irradiation for 40 min. Before the tribological test, the samples were placed in the fluid cell. The frequency method was used to determine the exact value of the normal spring constant (k_N) of the probe,[54] and the improved wedge calibration method was used to regulate the quantitative calibration of lateral force.[55] The loading force ranged from 100 to 400 nN, which was equivalent to the maximum contact stress varying from 35 to 55 MPa based on the Hertz equation for the ball-on-flat configuration.[56] The scan rate was 2 Hz. The value of the COF was calculated by dividing the lateral force (F_L) by the loading force (F_N). All of the tribological tests were repeated at different locations (area: 20×20 μm) on the silicon wafer at least three times to acquire the COF value. The COF values of MoS$_2$ and MoS$_2$-PDMPC with different concentrations (0.1, 0.5, and 1 mg mL^{-1}) under different pressures (35 to 55 MPa) were statistically compared.

Photothermal Conversion Properties of MoS$_2$-PDMPC-DS: The temperature changes and photothermal images of MoS$_2$ and MoS$_2$-PDMPC-DS under NIR laser (Leishi Co., Changchun, China) irradiation at 808 nm were captured by the NIR laser thermal imaging camera (FLIR T1040, Wilsonville, OR, USA) every 30 s. The temperature changes of MoS$_2$-PDMPC-DS (0.6 mg mL^{-1}) under different power densities (0.2, 0.4, 0.6, and 0.8 W cm^{-2}) of the NIR laser and different concentrations of MoS$_2$-PDMPC-DS under a constant NIR laser power density (1 W cm^{-2}) were recorded by a thermocouple (FST600-102, First rate, Changsha, China). To detect the thermal stability of MoS$_2$-PDMPC-DS nanosheets, an NIR laser (0.6 W cm^{-2}) was used to irradiate MoS$_2$-PDMPC-DS solution, then the irradiation was stopped until the solution returned to 25 °C. This laser off/on test was repeated for

4 times, and each laser irradiation time was 4 min. In this process, the thermocouples were employed to monitor and record temperature changes in the solution in real time.

Drug Loading and Photothermal Capacity-Induced Drug Release of MoS$_2$-PDMPC-DS: MoS$_2$, PDMPC, and DS were magnetically stirred overnight to obtain MoS$_2$-PDMPC-DS. The nanosheets were collected by centrifugation (8000 rpm, 10 min), and the absorbance of the supernatant was detected by UV–vis to determine the concentration of DS. The drug loading rate was calculated by dividing the mass of loaded DS by the mass of MoS$_2$-PDMPC-DS. The drug release experiment was conducted at 25 °C. The solution of MoS$_2$-PDMPC-DS in PBS was irradiated with an 808 nm NIR laser at a power density of 0.2 W cm^{-2} for 10 min, followed by 50 min intervals without NIR laser irradiation. Then, the MoS$_2$-PDMPC-DS solution was centrifuged (12000 rpm, 30 min) to obtain the supernatant, and the released DS was determined by measuring the absorbance of the supernatant using UV–vis. The MoS$_2$-PDMPC-DS solution was irradiated with the laser again, and the absorbance of the supernatant was measured. This process was repeated for 8 times.

Biocompatibility of MoS$_2$-PDMPC-DS and Macrophage Uptake: The cell study was approved by the Institutional Animal Care and Use Committee (IACUC), Peking University, China. Chondrocytes were extracted from the knee joints of Sprague Dawley (SD) rats (4–6 weeks) which were purchased from Si Pei Fu (Beijing) Biotechnology Co., Ltd., Beijing, China. The knee cartilage of the rats was cut into small fragments (<1 mm^3) and washed thoroughly with PBS three times. The tissue fragments were digested by collagenase II at 37 °C for 4 h, and then Dulbecco's modified Eagle's medium (DMEM, containing 10% FBS and 1% antibiotics) was added to terminate the digestion. Chondrocytes were cultured in a cell incubator (37 °C, 5% CO$_2$, and 95% humidity).

RAW 264.7 cells and chondrocytes were used as representative cells to evaluate the biocompatibility of MoS$_2$-PDMPC-DS. A CCK-8 assay was performed to detect the cytotoxicity of MoS$_2$-PDMPC-DS. RAW 264.7 cells and chondrocytes were seeded into 96-well plates (10^4 cells per well) and incubated overnight in the incubator (37 °C, 5% CO$_2$, and 95% humidity). The cells were co-cultured with MoS$_2$-PDMPC-DS solutions (0.2 mg mL^{-1}) for 24 h with or without NIR laser irradiation (808 nm, 0.2 W cm^{-2}). Then, 10 μL CCK-8 reagent was added to each well and incubated for 2 h. The absorbance of each well was read by a microplate reader (CMax Plus, Leica, Wetzlar, Germany) at a wavelength of 450 nm. The live/dead staining (Gibco, Grand Island, NY, USA) assay was employed to determine the biocompatibility of MoS$_2$-PDMPC-DS. RAW 264.7 cells and chondrocytes were seeded into 6-well plates (10^5 cells per well) and incubated overnight (37 °C, 5% CO$_2$, and 95% humidity). Afterward, the cells were co-cultured with MoS$_2$-PDMPC-DS solution for 24 h, dyed with PI (dead cell, red) and AM (living cell, green) for 20 min, and then imaged by a fluorescence microscope (OLYMPUS, U-RFL-T, Tokyo, Japan).

MoS$_2$ and MoS$_2$-PDMPC-DS were labeled with fluorescein O-methacrylate (MoS$_2$-PDM@F and MoS$_2$-PDMPC-DS@F) to evaluate cellular uptake behavior. Briefly, fluorescein O-methacrylate labeled PDMPC and PDM were synthesized by free radical polymerization similar to the preparation of PDMPC. The mass of monomers was 0.44 g of DMA, 0.59 g of MPC, and 0.016 g of fluorescein O-methacrylate for the preparation of PDMPC@F. The mass of monomers was 0.44 g of DMA and 0.016 g of fluorescein O-methacrylate for the preparation of PDM@F. Then, PDM@F and PDMPC@F were utilized to prepare MoS$_2$-PDM@F and MoS$_2$-PDMPC-DS@F. MoS$_2$-PDM@F and MoS$_2$-PDMPC-DS@F were co-cultured with macrophages for 4 h, and DAPI was added at 25 °C for 15 min. The cellular uptake of macrophages was observed using a confocal laser scanning microscope (CLSM, LEICA TCS SP8, Leica, Wetzlar, Germany). For flowcytometry, macrophages were treated with MoS$_2$-PDM@F or MoS2-PDMPC-DS@F as described above, and analyzed using a flow cytometer (LSRII, BD, NJ, USA).

In Vitro Anti-Inflammatory Effect of MoS$_2$-PDMPC-DS: RAW 264.7 cells were seeded in 48-well plates (2×10^4 cells per well) and incubated in the incubator (37 °C, 5% CO$_2$, and 95% humidity) overnight. Then,

5 µg mL^{-1} LPS was added to each well and incubated for 8 h to activate macrophages to produce inflammatory cytokines and mimic the inflammatory environment. PBS was added to remove excess LPS. MoS$_2$-PDMPC-DS and the corresponding content of DS were added and incubated at 37 °C for 24 h. The cells were divided into the control group, PBS group, DS group, and MoS$_2$-PDMPC-DS group. Each group included two subgroups clarified with or without NIR laser irradiation (808 nm, 0.2 W cm^{-2}) for 10 min. RAW 264.7 cells without LPS treatment were chosen as the control group. The cells were cultured overnight in a cell incubator (37 °C, 5% CO$_2$, and 95% humidity). The inflammatory factors (including TNF-α, IL-6, and IL-1β) of each group were quantified by ELISA kits.

Chondrocytes were seeded in 6-well plates (2×10^4 cells per well). To simulate an osteoarthritis microenvironment, 100 µM H$_2$O$_2$ was added to each well and incubated for 12 h. The chondrocyte grouping was the same as the macrophage grouping mentioned above. The RNA of the cells in each group was extracted with TRIzol reagent, and its purity and the corresponding concentrations were measured using a nanodrop spectrophotometer (ND-1000, Thermo Scientific,Waltham, MA, USA) via the absorbance at 260 and 280 nm. RNA was reverse transcribed into complementary deoxyribonucleic (cDNA) using a reverse transcription system kit. cDNA was amplified by qRT-PCR with an ABI 7500 Sequencing Detection System (Applied Biosystems, Waltham, MA, USA) and a SYBR Premix Ex Tag Kit. Specific primers were used to detect the expression levels of mRNAs, including Col2α, MMP1, TAC1 and β-actin, and all the factors were normalized to β-actin. The specific primer sequences were as follows:

β-actin: forward, 5′-CCCATCTATGAGGGTTACGC-3′; reverse, 5′-TTTAATGTCACGCACGATTTC-3′.

Col2α: forward, 5′-CTCAAGTCGCTGAACAACCA-3′; reverse, 5′-GTCTCCGCTCTTCCACTCTG-3′.

MMP1: forward, 5′-CACTCCCTTGGACTCACTCA-3′; reverse, 5′-CCCATATAAAGCCTGGATGC-3′.

TAC1: forward, 5′-TTGCAGAGGAAATCGGTGCC-3′; reverse, 5′-GAACTGCTGAGGCTTGGGTC-3′.

The mRNA expression levels of Col2α, MMP1 and TAC1 in each group were compared to evaluate the anti-inflammatory effect of MoS$_2$-PDMPC-DS on chondrocytes.

Fluorescence immunostaining of chondrocytes was performed to detect the expression of Col2α. Chondrocytes were seeded in 6-well plates (2×10^4 cells per well), and 100 µM H$_2$O$_2$ was added to each well and incubated for 12 h. Cell grouping was the same as the experiment mentioned above. The cells were incubated overnight and then fixed with 4% paraformaldehyde for 30 min. TritonX-100 (0.3%) was added for 30 min. Then, the cells were blocked with 10% goat serum at 25 °C for 1 h. Primary anti-Col2α monoclonal antibody (1:200 dilution) was added and incubated overnight at 4 °C, and fluorescent conjugated secondary antibody (1:200 dilution) was added and incubated for 1 h in the dark. DAPI was added at 25 °C for 15 min. Finally, confocal laser scanning microscopy was used to obtain immunofluorescence images.

Animal Experiment: The animal study was approved by the Institutional Animal Care and Use Committee (IACUC), Peking University, China. To clarify the photothermal conversion of MoS$_2$-PDMPC-DS in rat joint cavities, MoS$_2$-PDMPC-DS and normal saline were injected into the knee joints of the rats. After irradiation with an NIR laser for 10 min, the temperature changes and photothermal images in the joint cavity of the rats were acquired by an NIR photothermal camera.

MoS$_2$-PDMPC-DS@F and MoS$_2$-PDM@F were injected into the rat knee joint cavities, and the change in fluorescence intensity in the rat knee joint was observed with a small animal imager (Fluor Vivo, INDEC Bio Systems, Toronto, Ontario, Canada).

Eight-week-old SD male rats were divided into a control group (Con), osteoarthritis group (OA), NIR laser irradiation group (NIR), OA with NIR laser irradiation group (OA+NIR), DS treatment group (DS), DS with NIR laser irradiation group (DS+NIR), MoS$_2$-PDMPC-DS treatment group (MoS$_2$-PDMPC-DS), and MoS$_2$-PDMPC-DS with NIR laser group (MoS$_2$-PDMPC-DS+NIR), for a total of 8 groups ($n = 3$). The mode of administration was intra-articular injection. The original balance of knee joints of the rats was destroyed by ACLT and meniscectomy, and then the rats were placed on a small animal treadmill (SA101B, Sansibio, China) every other day to run at a speed of 15 m min^{-1} for 1 h to induce osteoarthritis in rats (Figure S12, Supporting Information). The knee joints were injected with DS or MoS$_2$-PDMPC-DS once a week and irradiated with an NIR laser every other day.

Imaging Manifestations of Animal Knee Joints: X-ray (eXpert DC, GENDEX, Hangzhou, China) and cone beam computed tomography (CBCT, PLX3000A, Xuemono, Beijing, China) of rat knee joints were performed at 2 and 4 weeks post-treatment. The joint space width of rat knee joints was measured with Mimics software according to CBCT images (Materialise, Shanghai, China) (Figure S13, Supporting Information). In addition, the rats were euthanized at 2 and 4 weeks after surgery, the right knee joint of the rat (including the knee joint and the proximal femur and tibia) was fixed, and the specimens were scanned and analyzed on a microcomputed tomography (micro-CT, SkyScan 1272, Bruker) system.

Histological Examination: The rats were euthanized, and the right knee joint of the rat was removed with a joint capsule. The samples were soaked in 4% paraformaldehyde for 48 h, and decalcified in 10% ethylenediaminetetraacetic acid (EDTA) at 37 °C in a constant temperature shaker for 2 weeks. The joint was embedded in paraffin, and tissue sections (thickness: 5 µm) were prepared for histological staining. Histological staining with HE and safranin-O fast green staining were performed, followed by tissue histopathological scoring (OARIS) based on cartilage damage and calcification. The content of relative GAG was quantified according to the results of safranin-O fast green staining by ImageJ software. To further detect the progression of osteoarthritis and cartilage degeneration, immunohistochemical staining was performed on rat knee joints, and Col2α, a protein that is closely related to osteoarthritis in cartilage, was used as a specific marker. Briefly, after the primary antibody against Col2α was incubated with the tissue sections at 4 °C overnight, the tissue sections were incubated with the secondary antibodies at room temperature for 2 h. The Col2α-positive cells were quantified by ImageJ software. For in vivo toxicity evaluation, HE staining of important viscera (heart, liver, spleen, lung, and kidney) tissues were performed.

Statistical Analysis: All experiments were repeated three times to ensure accuracy. The data are expressed as the mean ± SD. One-way analysis of variance (ANOVA) was used for comparison, and Games–Howell test was further used for post hoc multiple comparisons. Statistical significance is displayed as *$p < 0.05$, **$p < 0.01$, and ***$p < 0.001$. The statistical analysis was conducted by using SPSS statistical software (SPSS Inc., Chicago, IL, USA).

Supporting Information

Supporting Information is available from the Wiley Online Library or from the author.

Acknowledgements

Conflict of Interest

The authors declare no conflict of interest.

Data Availability Statement

The data that support the findings of this study are available from the corresponding author upon reasonable request.

[1] N. K. Arden, T. A. Perry, R. R. Bannuru, O. Bruyère, C. Cooper, I. K. Haugen, M. C. Hochberg, T. E. McAlindon, A. Mobasheri, J.-Y. Reginster, *Nat. Rev. Rheumatol.* **2021**, *17*, 59.

[2] Y. Xie, A. Zinkle, L. Chen, M. Mohammadi, *Nat. Rev. Rheumatol.* **2020**, *16*, 547.

[3] Y. Sun, Y. Han, Y. Dou, X. Gong, H. Wang, X. Yu, Q. Wang, Y. Wang, Y. Dai, F. Ye, W. Jin, H. Zhang, *Bioact. Mater.* **2022**, *14*, 120.

[4] C. G. Boer, K. Hatzikotoulas, L. Southam, L. Stefánsdóttir, Y. Zhang, R. C. de Almeida, T. T. Wu, J. Zheng, A. Hartley, M. Teder-Laving, A. H. Skogholt, C. Terao, E. Zengini, G. Alexiadis, A. Barysenka, G. Bjornsdottir, M. E. Gabrielsen, A. Gilly, T. Ingvarsson, M. B. Johnsen, H. Jonsson, M. Kloppenburg, A. Luetge, S. H. Lund, R. Mägi, M. Mangino, R. R. G. H. H. Nelissen, M. Shivakumar, J. Steinberg, H. Takuwa, et al, *Cell* **2021**, *184*, 4784.

[5] G. Bjornsdottir, L. Stefansdottir, G. Thorleifsson, P. Sulem, K. Norland, E. Ferkingstad, A. Oddsson, F. Zink, S. H. Lund, M. S. Nawaz, G. Bragi Walters, A. T. Skuladottir, S. A. Gudjonsson, G. Einarsson, G. H. Halldorsson, V. Bjarnadottir, G. Sveinbjornsson, A. Helgadottir, U. Styrkarsdottir, L. J. Gudmundsson, O. B. Pedersen, T. F. Hansen, T. Werge, K. Banasik, A. Troelsen, S. T. Skou, L. W. Thørner, C. Erikstrup, K. R. Nielsen, S. Mikkelsen, et al, *Nat. Commun.* **2022**, *13*, 634.

[6] Y. Hu, X. Chen, S. Wang, Y. Jing, J. Su, *Bone Res.* **2021**, *9*, 20.

[7] D. Yu, K. P. Jordan, K. I. E. Snell, R. D. Riley, J. Bedson, J. J. Edwards, C. D. Mallen, V. Tan, V. Ukachukwu, D. Prieto-Alhambra, C. Walker, G. Peat, *Ann. Rheum. Dis.* **2019**, *78*, 91.

[8] N. C. Butterfield, K. F. Curry, J. Steinberg, H. Dewhurst, D. Komla-Ebri, N. S. Mannan, A.-T. Adoum, V. D. Leitch, J. G. Logan, J. A. Waung, E. Ghirardello, L. Southam, S. E. Youlten, J. M. Wilkinson, E. A. McAninch, V. E. Vancollie, F. Kussy, J. K. White, C. J. Lelliott, D. J. Adams, R. Jacques, A. C. Bianco, A. Boyde, E. Zeggini, P. I. Croucher, G. R. Williams, J. H. D. Bassett, *Nat. Commun.* **2021**, *12*, 467.

[9] C. Zeng, J. Wei, M. S. M. Persson, A. Sarmanova, M. Doherty, D. Xie, Y. Wang, X. Li, J. Li, H. Long, G. Lei, W. Zhang, *Br. J. Sports Med.* **2018**, *52*, 642.

[10] C.-C. Szeto, K. Sugano, J.-G. Wang, K. Fujimoto, S. Whittle, G. K. Modi, C.-H. Chen, J.-B. Park, L.-S. Tam, K. Vareesangthip, K. K. F. Tsoi, F. K. L. Chan, *Gut* **2020**, *69*, 617.

[11] Y. Pan, S. Cao, A. S. Terker, J. Tang, K. Sasaki, Y. Wang, A. Niu, W. Luo, X. Fan, S. Wang, M. H. Wilson, M.-Z. Zhang, R. C. Harris, *Kidney Int.* **2022**, *101*, 79.

[12] C. Cadet, E. Maheu, *Ther. Adv. Musculoskelet. Dis.* **2021**, *13*, 1759720X211022149.

[13] K. Li, G. Yan, H. Huang, M. Zheng, K. Ma, X. Cui, D. Lu, L. Zheng, B. Zhu, J. Cheng, J. Zhao, *J. Nanobiotechnol.* **2022**, *20*, 38.

[14] D. J. Hunter, S. Bierma-Zeinstra, *Lancet* **2019**, *393*, 1745.

[15] B. R. da Costa, T. V. Pereira, P. Saadat, M. Rudnicki, S. M. Iskander, N. S. Bodmer, P. Bobos, L. Gao, H. D. Kiyomoto, T. Montezuma, M. O. Almeida, P.-S. Cheng, C. A. Hincapié, R. Hari, A. J. Sutton, P. Tugwell, G. A. Hawker, P. Jüni, *BMJ* **2021**, *375*, n2321.

[16] A. P. Ijzerman, K. A. Jacobson, C. E. Müller, B. N. Cronstein, R. A. Cunha, *Pharmacol. Rev.* **2022**, *74*, 340.

[17] Y. Lu, J. Chen, L. Li, Y. Cao, Y. Zhao, X. Nie, C. Ding, *J. Nanobiotechnol.* **2022**, *20*, 89.

[18] J. Gao, Z. Xia, H. B. Mary, J. Joseph, J. N. Luo, N. Joshi, *Trends Pharmacol. Sci.* **2022**, *43*, 171.

[19] R. Xie, H. Yao, A. S. Mao, Y. Zhu, D. Qi, Y. Jia, M. Gao, Y. Chen, L. Wang, D.-A. Wang, K. Wang, S. Liu, L. Ren, C. Mao, *Nat. Biomed. Eng.* **2021**, *5*, 1189.

[20] N. G. Kotla, S. R. Bonam, S. Rasala, J. Wankar, R. A. Bohara, J. Bayry, Y. Rochev, A. Pandit, *J. Controlled Release* **2021**, *336*, 598.

[21] H. Chen, T. Sun, Y. Yan, X. Ji, Y. Sun, X. Zhao, J. Qi, W. Cui, L. Deng, H. Zhang, *Biomaterials* **2020**, *242*, 119931.

[22] Y. Lei, X. Wang, J. Liao, J. Shen, Y. Li, Z. Cai, N. Hu, X. Luo, W. Cui, W. Huang, *Bioact. Mater.* **2022**, *16*, 472.

[23] Y. Lei, Y. Wang, J. Shen, Z. Cai, C. Zhao, H. Chen, X. Luo, N. Hu, W. Cui, W. Huang, *Sci. Adv.* **2022**, *8*, eabl6449.

[24] Y. Han, J. Yang, W. Zhao, H. Wang, Y. Sun, Y. Chen, J. Luo, L. Deng, X. Xu, W. Cui, H. Zhang, *Bioact. Mater.* **2021**, *6*, 3596.

[25] N. Rohaizad, C. C. Mayorga-Martinez, M. Fojtů, N. M. Latiff, M. Pumera, *Chem. Soc. Rev.* **2021**, *50*, 619.

[26] Z.-L. Lei, B. Guo, *Adv. Sci.* **2022**, *9*, 2102924.

[27] J. Liu, F. Li, J. Zheng, B. Li, D. Zhang, L. Jia, *J. Nanobiotechnol.* **2019**, *17*, 78.

[28] N. Dalila R, M. K. Md Arshad, S. C. B. Gopinath, W. M. W. Norhaimi, M. F. M. Fathil, *Biosens. Bioelectron.* **2019**, *132*, 248.

[29] X. Chen, C. Bartlam, V. Lloret, N. M. Badlyan, S. Wolff, R. Gillen, T. Stimpel-Lindner, J. Maultzsch, G. S. Duesberg, K. C. Knirsch, A. Hirsch, *Angew. Chem., Int. Ed.* **2021**, *60*, 13484.

[30] G. Deokar, D. Vignaud, R. Arenal, P. Louette, J. F. Colomer, *Nanotechnology* **2016**, *27*, 075604.

[31] Y. Zhao, C. Wei, X. Chen, J. Liu, Q. Yu, Y. Liu, J. Liu, *ACS Appl. Mater. Interfaces* **2019**, *11*, 11587.

[32] A. Vanossi, C. Bechinger, M. Urbakh, *Nat. Commun.* **2020**, *11*, 4657.

[33] J. Hao, G. Song, T. Liu, X. Yi, K. Yang, L. Cheng, Z. Liu, *Adv. Sci.* **2017**, *4*, 1600160.

[34] L. M. Guiney, X. Wang, T. Xia, A. E. Nel, M. C. Hersam, *ACS Nano* **2018**, *12*, 6360.

[35] Z. Yang, Z. Guo, C. Yuan, *Wear* **2019**, *102919*, 432.

[36] O. O. Ajayi, A. Erdemir, J. H. Hsieh, R. A. Erck, G. R. Fenske, *Lubr. Eng.* **1992**, *48*, 584.

[37] V. Donadei, H. Koivuluoto, E. Sarlin, P. Vuoristo, *Polymers* **2022**, *14*, 303.

[38] F. Veronesi, G. Boveri, M. Raimondo, *Materials* **2019**, *12*, 787.

[39] Y. Shen, Y. Wu, J. Tao, C. Zhu, H. Chen, Z. Wu, Y. Xie, *ACS Appl. Mater. Interfaces* **2019**, *11*, 3590.

[40] Y. Yin, G. Zhang, X. Xu, P. Zhao, L. Ma, *R. Soc. Open Sci.* **2021**, *8*, 210565.

[41] L. Ma, A. Gaisinskaya-Kipnis, N. Kampf, J. Klein, *Nat. Commun.* **2015**, *6*, 6060.

[42] J. Klein, *Science* **2009**, *323*, 47.

[43] C. Dong, C. Yuan, L. Wang, W. Liu, X. Bai, X. Yan, *Sci. Rep.* **2016**, *6*, 35023.

[44] Z. Zasłona, E. Flis, M. Wilk, R. Carroll, E. Palsson-McDermott, M. Hughes, C. Diskin, K. Banahan, D. G. Ryan, A. Hooftman, A. Misiak, J. Kearney, G. Lochnit, W. Bertrams, T. Greulich, B. Schmeck, O. J. McElvaney, K. H. G. Mills, E. C. Lavelle, M. Wygrecka, E. M. Creagh, L. A. J. O'Neill, *Nat. Commun.* **2020**, *11*, 1055.

[45] X. Wang, B. Yao, Y. Wang, X. Fan, S. Wang, A. Niu, H. Yang, A. Fogo, M. Zhang, R. Harris, *Diabetes* **2017**, *66*, 494.

[46] B. Luan, Y. Yoon, J. Lay, K. Kaestner, S. Hedrick, M. Montminy, *Proc. Natl. Acad. Sci. USA* **2015**, *112*, 15642.

[47] J. Yin, H. Zeng, K. Fan, H. Xie, Y. Shao, Y. Lu, J. Zhu, Z. Yao, L. Liu, H. Zhang, B. Luo, X. Wang, C. Zeng, X. Bai, H. Zhang, D. Cai, *Cell Death Dis.* **2022**, *13*, 567.

[48] M. Ahmed, A. Mehmood, F. Bhatti, S. Khan, S. Riazuddin, *Osteoarthr. Cartil.* **2014**, *22*, 1894.

[49] J. Lu, Y. Peng, J. Zou, J. Wang, S. Lu, T. Fu, L. Jiang, C. Zhang, J. Zhang, *Cartilage* **2021**, *13*, 1030S.

[50] R. Oğuz, M. Belviranlı, N. Okudan, *Cartilage* **2021**, *13*, 1791S.

[51] C. Xu, K. Pu, *Chem. Soc. Rev.* **2021**, *50*, 1111.

[52] Q. Zhang, Y. Ren, Y. Mo, P. Guo, P. Liao, Y. Luo, J. Mu, Z. Chen, Y. Zhang, Y. Li, L. Yang, D. Liao, J. Fu, J. Shen, W. Huang, X. Xu, Y. Guo, L. Mei, Y. Zuo, J. Liu, H. Yang, R. Jiang, *Cell Res.* **2022**, *32*, 461.

[53] W. Zhao, H. Wang, Y. Han, H. Wang, Y. Sun, H. Zhang, *ACS Appl. Mater. Interfaces* **2020**, *12*, 51236.

[54] Y. Song, S. Wu, L. Xu, X. Fu, *Sensors* **2015**, *15*, 5865.

[55] C. Dziekoński, W. Dera, D. M. Jarząbek, *Ultramicroscopy* **2017**, *182*, 1.

[56] Y. Zheng, J. Yang, J. Liang, X. Xu, W. Cui, L. Deng, H. Zhang, *Biomacromolecules* **2019**, *20*, 4135.